*J. Fluid Mech.* (1974), *vol.* 64, *part* 4, *pp.* 645–678
*Printed in Great Britain*



# Some turbulent/non-turbulent properties of the outer intermittent region of a boundary layer

By THOMAS B. HEDLEY† AND JAMES F. KEFFER
Department of Mechanical Engineering, University of Toronto

(Received 28 December 1972)

A detailed study of the intermittency in the outer region of a flat-plate turbulent boundary layer has been carried out using digital sampling and processing techniques. Conditional averages are used to generate mean and fluctuating components for the turbulent and non-turbulent zones of fluid. More particularly, point averages of these variables, taken with reference to the instantaneous position of the turbulent/non-turbulent interface, have been made to show the distribution of various quantities through the turbulent front. The results indicate that significant differences exist at leading and trailing edges of the turbulent bursts and a more complete picture of the motion of an average large eddy is deduced.

## 1. Introduction

In the companion paper (Hedley & Keffer 1974) methods for determing when the intermittent region of a shear flow could be considered turbulent or non-turbulent were examined. A technique was proposed for making such decisions and a physical rationale advanced to justify the procedure. In this present paper, we apply the turbulent decision methods to a simple flat-plate turbulent boundary layer. The reasons for choosing this flow are varied. First, there is a considerable amount of data available in the literature on the intermittent structure, which can be used as an overall check on our results (Kovasznay, Kibens & Blackwelder 1970; Antonia & Bradshaw 1971; Antonia 1972). This body of information is not comprehensive, however. In particular, the details of the interfacial behaviour, that is, the explicit evaluation of variables across the turbulent/non-turbulent front, has not been made. We have extended our measurements to include this aspect, employing on-line digital data sampling and processing techniques. The use of digital computer methods has enabled us to take the necessary ensemble averages, which would have been difficult or perhaps impossible by conventional analog methods.

Furthermore, it has been realized recently that the simple boundary-layer flow exhibits some singularly interesting features. The presence of the wall ensures that a viscous-dominated region will exist, viz. the viscous sublayer. Recent experimental investigations (Kim, Kline & Reynolds 1971; Corino & Brodkey 1969) have revealed that large-scale random bursting originates from within

† Present address: Hatch Associates, Toronto.

this region, ejecting fluid into the mid-zone in a predictable but complicated sequence of events. Apparently this process is fundamental to the production of turbulence although what in particular triggers this bursting is still an open question. Narahari Rao, Narasimha & Narayanan (1971) have been able to show that these bursts can be correlated with the active periods of turbulence detected with narrow band-pass filters, over the complete depth of the boundary layer. Both the interval between the viscous-sublayer eruptions and the spacing between the active periods displayed a lognormal frequency distribution. In our present investigation, we carry this further, showing that the frequency of the smaller turbulent and non-turbulent zones in the outer intermittent region of the boundary layer is also lognormal. From this it might seem that there is a connexion between the inner wall region and the outer entrainment of fluid by the intermittent bursts into the free stream. This speculation is discussed in later sections.

## 2. Experimental procedure

### 2.1. *The generation of the boundary layer*

The investigation was carried out in the low turbulence wind tunnel of the Department of Mechanical Engineering at the University of Toronto. This is a closed-return tunnel with a test section $0{\cdot}9 \times 1{\cdot}2$ m and $4{\cdot}6$ m in length. Tapered fillets compensate for boundary-layer growth, producing a negligibly small streamwise pressure gradient. The existence of smoothing screens and a large contraction prior to the test section ensures a very low background level of turbulence, of the order of 0·0005 based on the longitudinal fluctuation intensity. A remote-controlled servo system allows positioning of probes in the test section to an accuracy of 0·005 mm in the two lateral directions and to within 0·05 mm in the streamwise direction.

To generate a typical two-dimensional boundary layer an aluminium plate was supported near the mid-plane of the tunnel, extending from wall to wall. The first 150 mm were shaped to give a near-elliptical leading edge. Number 16 garnet paper was glued along the first 610 mm of the plate. This served to trip the flow, resulting in an artificially thickened boundary layer. The method was essentially the same as that used by Klebanoff & Diehl (1953). A comparison of the present flow with that of others indicates that our developed boundary layer is generally similar to a natural transition layer. The wake region, as seen in figure 1, however, was smaller than for a normal equilibrium boundary layer and it is probable that the artificial transition had a residual effect. Our tests were carried out at a single station, 3·5 m from the leading edge of the plate. The mean characteristics of the flow at this point are given in table 1. The nominal thickness is rather high compared with the displacement and momentum thicknesses although both the shape parameter and the shear stress coefficient agree with published data. The slightly favourable pressure gradient of 0·020 was higher than those of either Kovasznay *et al.* (1970) or Gupta & Kaplan (1972), which were 0·012 and 0·004 respectively. The two-dimensionality of the layer was checked by measuring the $\overline{uw}$ component of the Reynolds stress at a number

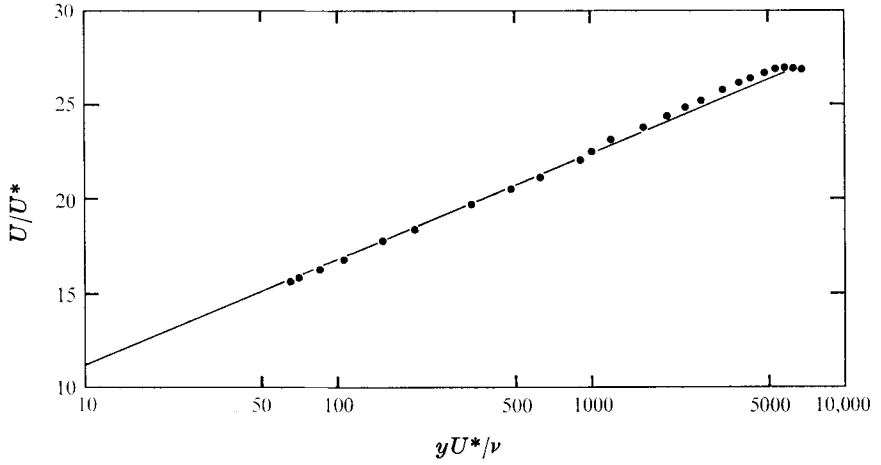


FIGURE 1. Boundary-layer velocity profile 3·5 m from leading edge of the plate.

of transverse stations. This was effectively zero except in the boundary-layer regions along the walls of the tunnel.

| | |
|---|---|
| Free-stream velocity | $U_\infty = 15{\cdot}24$ m/s |
| Nominal thickness (99 % point) | $\delta = 139{\cdot}7$ mm |
| Displacement thickness | $\delta_1 = 12{\cdot}60$ mm |
| Momentum thickness | $\delta_2 = 9{\cdot}73$ mm |
| Shape parameter | $H = 1{\cdot}30$ |
| Reynolds numbers | $Re = U_\infty \delta/\nu = 138\,000$ |
| | $Re_{\delta_2} = U_\infty \delta_2/\nu = 9700$ |
| Friction velocity | $U^*/U_\infty = 0{\cdot}037$ |
| Shear stress coefficient | $C_f = 0{\cdot}00274$ |
| Pressure gradient | $\frac{\delta_2 U_\infty}{U^{*2}} \frac{dU}{dx} = 0{\cdot}020$ |
| At $y/\delta = 1{\cdot}0$ | $y^+ = yU^*/\nu = 5{\cdot}106$ |

TABLE 1. Characteristics of the boundary layer

### 2.2. *Data acquisition*

DISA model 55A01 constant-temperature anemometers with platinum-plated tungsten X-wires (of length 1·2 mm and diameter 5 $\mu$m) were used at an overheat ratio $(R_w - R_g)/R_g$ of 0·8. $R_w$ is the operating resistance and $R_g$ the cold resistance of the wire. Wire sensitivities did not have to be matched because of the way in which the signal was sampled and processed (see §2.3).

Analog voltage signals from the two anemometers were low-pass filtered to 5000 Hz separately using identical filters. Then, each signal was digitally sampled by means of a Remote Analog Digital Data Terminal (RADDT), model IBM 3963, at $10^{-4}$ s intervals. This unit is designed to sample up to 8 analog (or digital) channels, to convert the readings to digital (or analog) values and to transmit the data in a 17 bit parallel mode to an IBM system 360, model 44 computer which directs the data acquisition. A schematic diagram of the operation is shown in

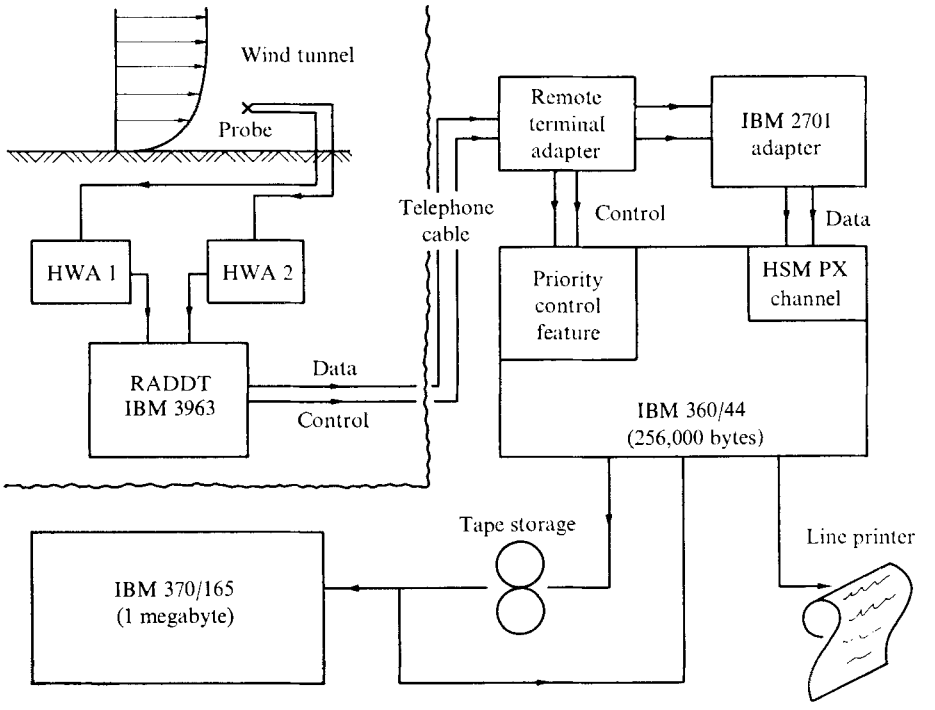


FIGURE 2. Schematic sketch of data acquisition system.

| | |
|---|---|
| Number of dual-purpose channels (analog or digital) | 4 |
| Number of analog-only channels | 4 |
| Channel resolution | 12 bits plus sign |
| Channel address | 3 bits plus parity |
| Analog input range | ± 10 V protected to ± 125 V |
| Analog input system accuracy | ± 0·05 % F.S. (10 V)<br>± 0·05 % of reading<br>± 0·033 % F.S./°C<br>± ½ LSB |
| Analog input impedance at d.c. | 10 MΩ |
| Analog input charging time constant | 100 ns max. |
| Analog input frequency response | D.c. to 10 kHz (for specified accuracy) |
| Input sampling aperture time | 50 ns |
| Analog input settling time, full-scale step | 10 μs |
| Digital input logic levels | 0 = 0–0·15 V or open<br>1 = 2·5–30 V protected to ± 125 V |
| Channel multiplexing rate | 20 000 channels/s maximum |
| Channel multiplexing mode | Fixed sequence (number of channels scanned is selected on front panel) |
| Internal clock frequencies | 20 000 Hz, 10 000 Hz, 5000 Hz, 2500 Hz, 1250 Hz, 625 Hz, 312 Hz, 156 Hz |

TABLE 2. RADDT performance specifications

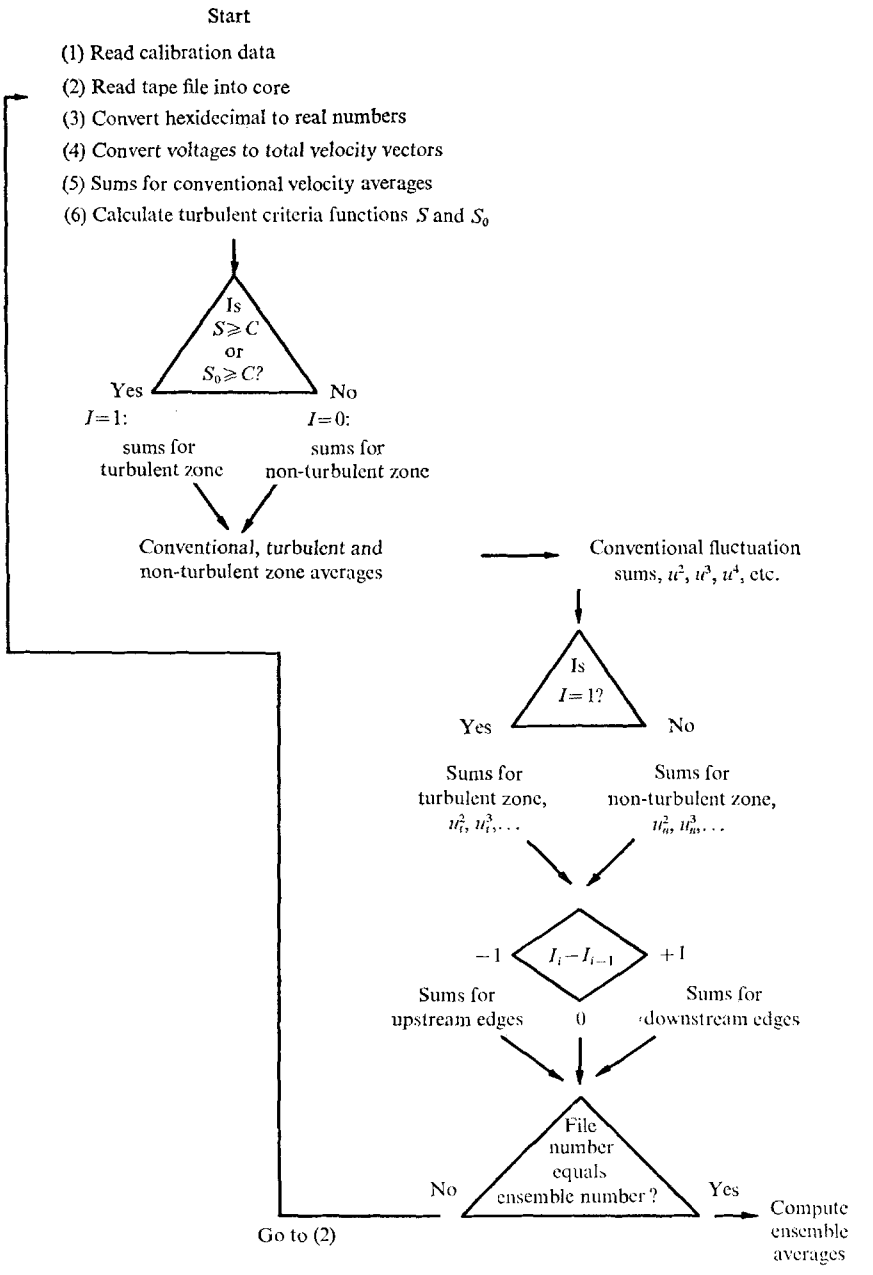


FIGURE 3. Flow chart illustrating data processing.

figure 2. Telephone cables connect the remote terminal through an IBM 2701 Adapter to a High Speed Multiplex (HSMP) channel of the 360–44 at the Computer Centre. At the Central Processing Unit (CPU) the data can be stored in binary form on magnetic tape, in which case processing would be carried out later, normally on an IBM system 370, model 165. Alternatively it can be processed immediately on the 360–44. The choice is governed by the particular CPU

program called into play by the user program. Limited control at the RADDT is available through five interrupt or control push buttons. The actual rate of data sampling and transfer, 156–20 000 samples/s, is controlled by an internal clock in the RADDT. The performance specifications are listed in table 2.

### 2.3. *Processing the information*

FORTRAN IV programs were used in processing the digital data. Some assembly-language subroutines, available at the Computing Centre, were called for tape handling and binary conversion. The magnetic tapes were read into the computer core and converted into real-number arrays of 16 000 elements. These voltage-read elements $E$, which alternately come from each of the two wires of the $X$-probe at $\frac{1}{2} \times 10^{-4}$ s intervals, were converted individually to effect cooling velocities $U_e$, through the basic equation

$$E^2 R_w/(R_w - R_g) = A + BU_e^n,$$

where $A$, $B$ and $n$ are experimental coefficients, determined for each wire. If second- and higher-order terms are ignored, the cooling velocities for each wire are related to the streamwise and transverse components by

$$U_{e1} = C_1 U + D_1 V, \quad U_{e2} = C_2 U + D_2 V,$$

where the constants $C$ and $D$ are functions of wire inclination. Although $U_{e1}$ and $U_{e2}$ are separated in real time by $\frac{1}{2} \times 10^{-4}$ s, we assumed them to be coincident. Thus a simultaneous solution for each pair gives the instantaneous values of $U$ and $V$ every $10^{-4}$ s. The sequential nature of the sampling produces an inevitable uncertainty in the results. The present lag time between pairs of data points, however, is only about a tenth of the smoothing time for the signal processing (Hedley & Keffer 1974), and it was felt that the error was of secondary importance. The various operations of producing a criterion function to identify the turbulence and, subsequently, the execution of conditional averaging of the signals can then be carried out. The flow chart in figure 3 gives details of the procedure.

### 2.4. *Stability of the data*

The period required for a finite-time average of a function $U(t)$ to reach a value within $\epsilon$ of its true ensemble average is (Lumley & Panofsky 1964, p. 37)

$$T_r = 2 \frac{\langle u^2 \rangle}{\langle U^2 \rangle} \frac{T_i}{\epsilon^2},$$

where $u = U - \langle U \rangle$ and $T_i$ is the integral scale of $u$. The length of record or the number of arrays processed was chosen on the basis of stability of the fourth moment of the $u$ fluctuations, the highest moment computed. For the fourth moment of a Gaussian variable, the above time period becomes

$$T_r = \tfrac{64}{3} T_i/\epsilon^2.$$

In an intermittent region of the flow, zone averages will accumulate in proportion to the product of the intermittency fraction $\bar{I}$ and the period of integration. Thus the length of record should be modified by $\bar{I}$, i.e. to $T_r/\bar{I}$. Point averages with respect to the position of the turbulent interface accumulate at the rate

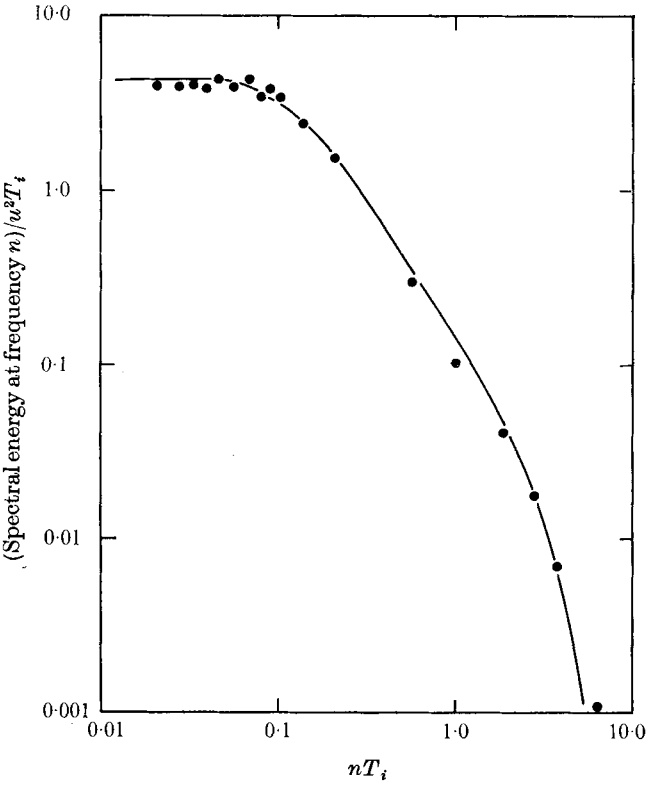


FIGURE 4. Spectrum of kinetic energy of streamwise fluctuating components; $y/\delta = 0{\cdot}57$. ●, present results; ——, Klebanoff & Diehl (1953).

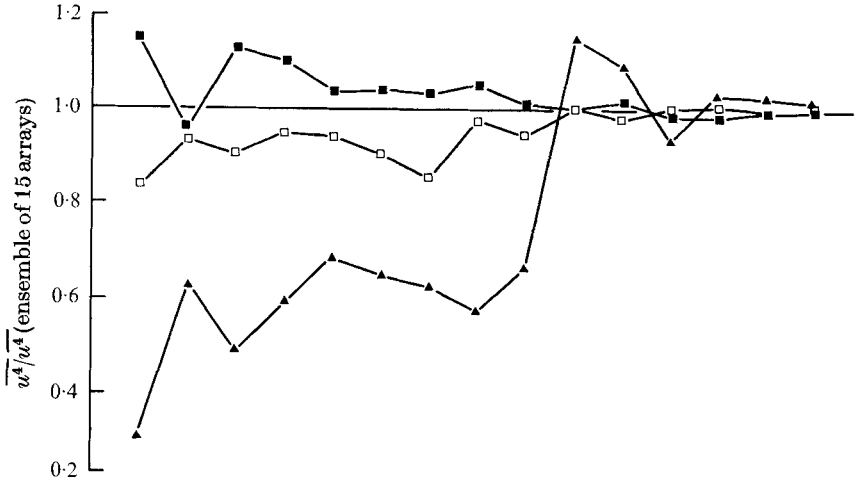


FIGURE 5. Test of stability based on computation of fourth moments for 15 arrays of data. ■, $\bar{I} = 0{\cdot}51$; □, $\bar{I} = 0{\cdot}89$; ▲, $\bar{I} = 0{\cdot}10$.

$f_\Lambda$, the frequency of occurrence of the turbulent zones. Actually one requires only one data point within every two integral scales to represent the statistics accurately (Sheih, Tennekes & Lumley 1971) and so the required sampling rate for point-averaged quantities should be of the order of $T_r/2\bar{I}f_\Lambda T_i$.

In lieu of a direct measurement of $T_i$ an estimate based on the peak of the energy spectrum may be substituted (Sheih *et al.* 1971). In our present situation, the spectrum showed a peak at approximately 500 Hz (figure 4). We thus chose $T_i = 0{\cdot}002$ s. As a reasonable error, $\epsilon$ was taken as 0·05, which gave $T_r = 18$ s. The ratio of the apparent integral time scale to the sampling interval was thus $T_i/\Delta T = 20$ and that of the actual record length to the sampling interval $T_r/\Delta T = 180000$. Actually, the convergence of the fourth moment, shown for 15 arrays of data in figure 5 (approximately 12 s), was thought to be sufficient and this was the final choice for the experiments. We therefore processed 180000 voltage pairs at $10^{-4}$ s separation to give the desired statistics at each experimental location. In terms of point averages this represented 1000 to 3000 items of data depending upon the particular value of $f_\Lambda$. The crossing frequency is of course a flow variable.

## 3. Results

There is no general agreement on the symbolism to represent the various averages in a conditionally sampled turbulent flow. Our particular choice, given in table 3, is a compromise but essentially follows the practice introduced by Kovasznay *et al.* (1970).

### 3.1. *The distribution of turbulent/non-turbulent fluid*

The complexity of the shape of the interface is evident from even a cursory examination of the flow. The large bulges and indentations are pre-eminent features. Corrsin & Kistler (1955) remarked that a study of the interface position $Y(x,t)$ with a single probe has the peculiar feature that at no time is this function directly available to us. As a result the standard techniques of analysis such as correlations and probability densities cannot be used. However, one can study the on/off periods of turbulence. By adopting the frozen-flow Taylor approximation, these time intervals can be considered equivalent to space intervals with lengths measured in the direction of the mean convection velocity. The indicator function $I(x,y,t)$, which is defined as zero when the flow is non-turbulent and unity when turbulent, is essentially a random square wave and this reflects directly time periods $T_t$ of the turbulent bursts and the corresponding periods $T_n$ of quiescent flow. Thus the statistical properties of $I(x,y,t)$ are those of the approximate zone widths $L_t = U_\infty T_t$ and $L_n = U_\infty T_n$.

The intermittency factor $\bar{I}$ is merely equivalent to the proportion of time a fixed probe would find itself in fully turbulent fluid. Ignoring differences in convection velocity across the bulges, the distribution of $\bar{I}$ will then identify the proportion of space occupied by turbulent fluid. The variation of the intermittency factor across the boundary layer (figure 6) is essentially that found by previous workers (Corrsin & Kistler 1955; Fiedler & Head 1966; Kovasznay *et al.* 1970).

| | |
|---|---|
| $P[\ ]$ | the probability of |
| $\overline{Q}$ | conventional time average |
| $\overline{\overline{Q}}$ | turbulent zone average (conditional) |
| $\tilde{\overline{Q}}$ | non-turbulent zone average (conditional) |
| $\hat{Q}$ | point average (conditional) |
| $\langle Q \rangle$ | ensemble average |
| $q(r,t) = Q(r,t) - \overline{Q}(r)$ | |
| $q_t(r,t) = Q(r,t) - \overline{\overline{Q}}(r)$ | |
| $q_n(r,t) = Q(r,t) - \tilde{\overline{Q}}(r)$ | |
| $q_p(r,t) = Q(r,t) - \hat{Q}(r)$ | |
| $\overline{q^2}, \overline{\overline{q_t^2}}, \tilde{\overline{q_n^2}}, \hat{q_p^2}$ | appropriate intensities |

TABLE 3. Definition of operations

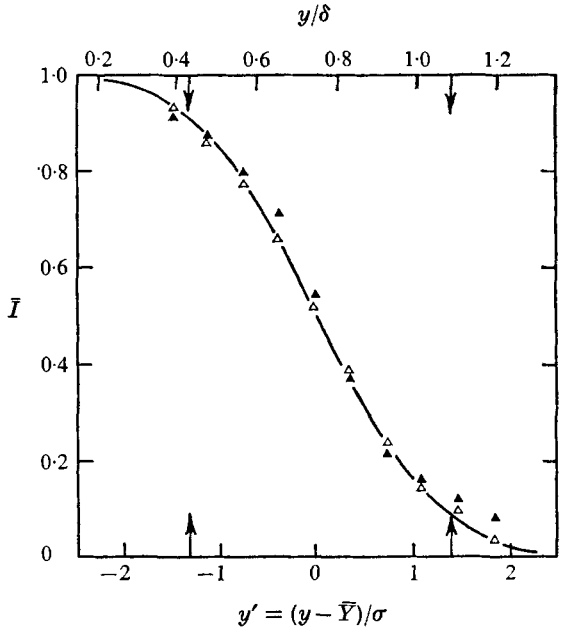


FIGURE 6. Distribution of the intermittency fraction. △, $\bar{I}$ determined directly ; ▲, determined from flatness factor of $\partial u/\partial t$; ——, normal distribution.

$Y$ is the lateral position of the interface and $\overline{Y}$ is defined as the point where $\bar{I} = 0{\cdot}5$. For convenience, the 10 and 90% intermittency points ($\bar{I} = 0{\cdot}10$ and $0{\cdot}90$) are marked by arrows on this and subsequent figures. An indirect measure of $\bar{I}$ using the flatness factor of $\partial u/\partial t$, after Townsend (1948), is included as well. The results are seen to be comparable except at the extreme outer edge of the flow. This is evidence that the structure of turbulence within the turbulent bursts in the

| | $\overline{Y}$ (mm) | $\sigma$ (mm) | $\overline{Y}/\delta$ | $\sigma/\delta$ |
|---|---|---|---|---|
| Present results | 103·3 | 33·0 | 0·75 | 0·24 |
| Kovasznay *et al.* (1970) | 80·0 | 14·4 | 0·80 | 0·15 |
| Antonia & Bradshaw (1971) | 51·2 | 21·6 | 0·64 | 0·27 |
| Klebanoff (1955) | — | — | 0·78 | 0·14 |
| Corrsin & Kistler (1955) | 71·2 | 12·5 | 0·80 | 0·14 |

TABLE 4. Interface statistics

outermost regions differs from that deep within the fully turbulent fluid. Indeed, Kennedy & Corrsin (1961) showed that a high flatness factor may be a necessary but not sufficient condition to guarantee that a particular flow is intermittent.

A comparison of the interface statistics with some previous work is shown in table 4. The present results are essentially Gaussian with $\overline{Y}/\delta = 0{\cdot}75$ and a standard deviation of $= \sigma/\delta\, 0{\cdot}24$. This spread is larger than might be expected for a normal boundary layer and comparable with the value obtained by Antonia & Bradshaw (1971), who examined the reattached flow downstream from a step. This is further evidence that our boundary layer was still under the influence of the artificial transition zone and not completely in equilibrium.

From an engineering point of view, the nominal thickness of the boundary layer is an important parameter. In an examination of the outer structure, however, the mean position of the interface is more significant. For this reason we have plotted the results in terms of the non-dimensional co-ordinate

$$y' = (y - \overline{Y})/\sigma.$$

The conventional representation, using $y/\delta$, is included as well for comparison.

A further comment on the uniqueness of $\bar{I}$ is illustrative. A simple analysis will show that identical turbulent fractions can be measured for different physical distributions of the turbulent fluid. As an example, frequently occurring short zones can produce the same result as a smaller number of infrequently changing large zones. We therefore tried to determine exactly how the zone widths were distributed. To accomplish this, the velocity records were scanned, the time periods of the zones were measured and the corresponding probability density functions for $L_t$ and $L_n$ were generated. These distributions were measured at various positions through the boundary layer. The results presented in figure 7 show that the broad spectra of zone widths tend to peak for small values. The general shape of the distributions and the trends as a function of the level of intermittency are similar to those reported by Corrsin & Kistler (1955).

The above authors showed that the density functions of $L_t$ and $L_n$ must be linear near the origin when $Y(t)$ is differentiable. This aspect together with the observed shape of the distributions suggests that a lognormal function might fit the data. This hypothesis was tested with the results shown in figure 8. The straight-line portions indicate that the spatial domains for both turbulent and non-turbulent fluid are distributed lognormally for the smaller zone widths. For values of $L$ greater than about $0{\cdot}06\overline{Y}$, there is an increasing departure from this fit, i.e. a deficiency of large widths.

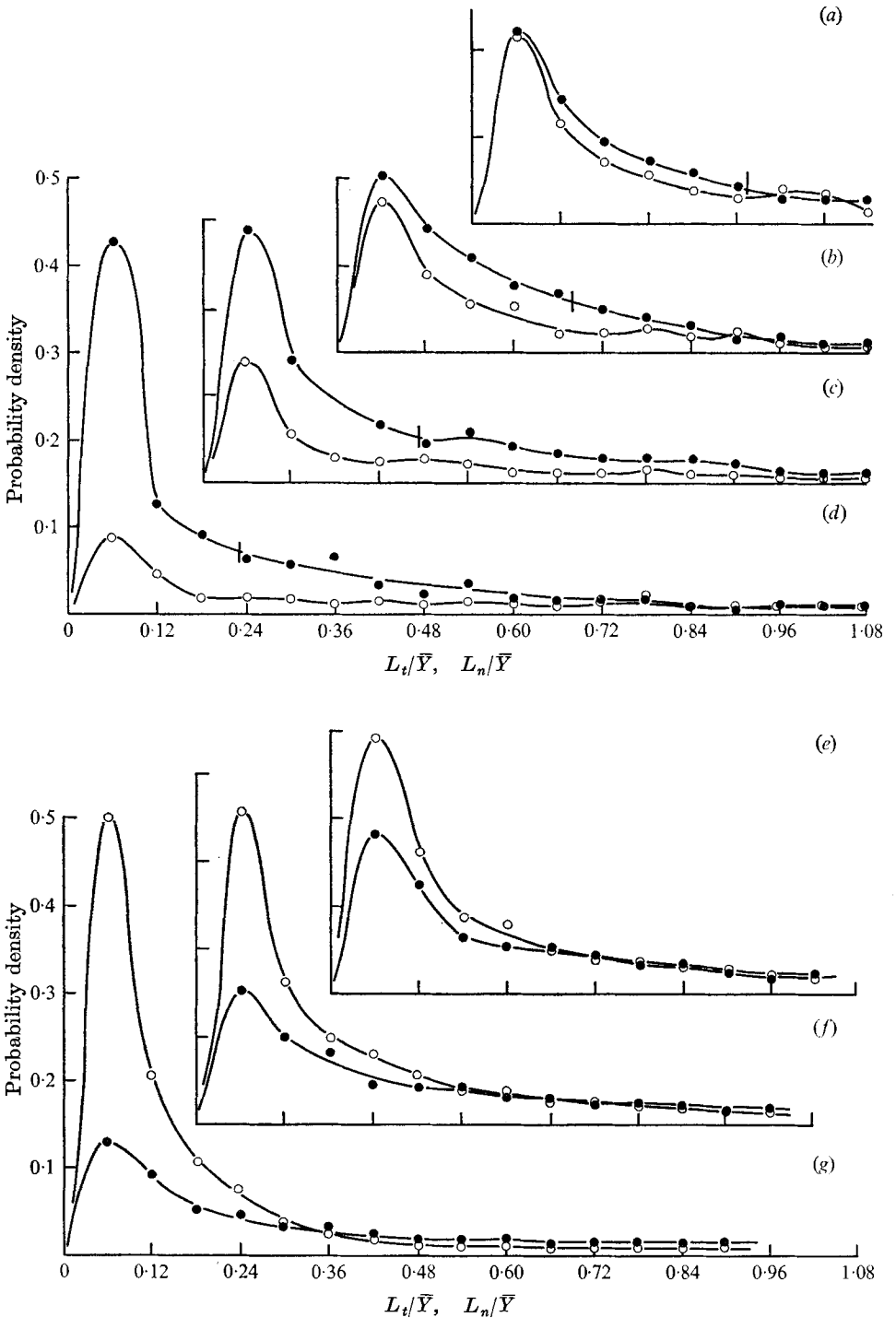


FIGURE 7. Probability density functions of zone widths. ●, turbulent zones; ○, non-turbulent zones. (*a*) $\bar{I} = 0{\cdot}38$. (*b*) $\bar{I} = 0{\cdot}24$. (*c*) $\bar{I} = 0{\cdot}10$. (*d*) $\bar{I} = 0{\cdot}04$. (*e*) $\bar{I} = 0{\cdot}66$. (*f*) $\bar{I} = 0{\cdot}78$. (*g*) $\bar{I} = 0{\cdot}93$.

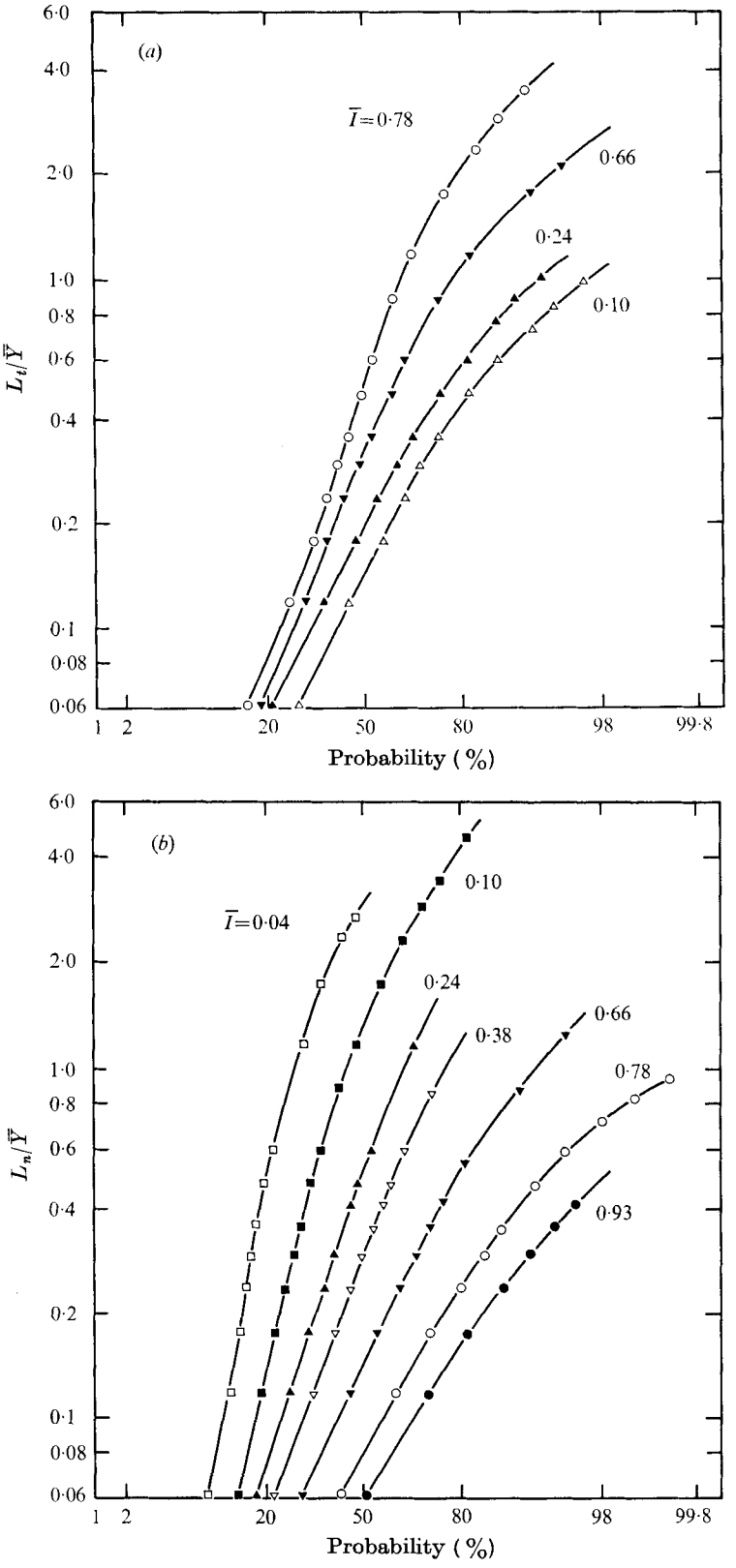


FIGURE 8. Probability density functions of (*a*) turbulent and (*b*) non-turbulent zone widths.

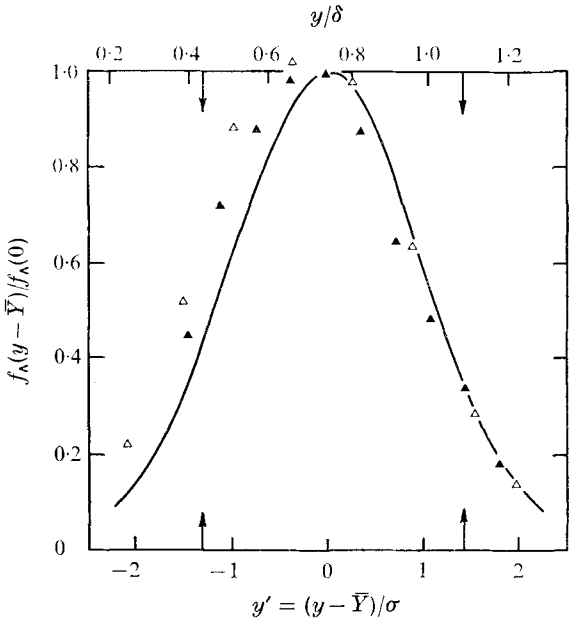


FIGURE 9. Frequency distribution of turbulent bulges. ▲, present results; △, Kovasznay *et al.* (1970); ——, normal distribution.

The indicator function $I(x, y, t)$ gives some insight into the way in which the turbulent fluid is distributed although the interpretation cannot be precise unless some restrictions are placed upon the shape of the interface. For example we may assume that folding of the front does not occur. Thus $Y(x, t)$ is single valued in time. As a consequence there will be a one-to-one correspondence between $\bar{I}(x, y)$ and $Y(x, t)$ viz.

$$\bar{I}(x, y) = P[y < Y(x, t) < \infty].$$

This assumption effectively demands that the interface position be normally distributed. Townsend (1966) noted that, if the surface displacement $Y - \overline{Y}$ and its gradient $\partial Y/\partial x$ were statistically independent and normally distributed, then the equation of the interface would take the form

$$F(Y) = \frac{1}{2\pi}\left\{\frac{\langle(\partial Y/\partial x)^2\rangle}{\langle(Y-\overline{Y})^2\rangle}\right\}^{\frac{1}{2}} \exp -\frac{1}{2}\left\{\frac{\langle(Y-\overline{Y})^2\rangle}{\langle(Y-\overline{Y})^2\rangle}\right\}.$$

This was tested at various positions across the layer by measuring

$$f_\Lambda \equiv (\langle L_t\rangle + \langle L_n\rangle)^{-1},$$

the average number of turbulent bursts or bulges per second. (We note that the number of occurrences of $Y$ would be twice this value since two crossings are required to define a burst.) The results given in figure 9 indicate a non-Gaussian behaviour in that there is a noticeable skewness to the distribution. Data from Kovasznay *et al.* (1970) also show this trend. Apparently the interfacial surface area is greater inside the point $\overline{Y}$ than beyond and we can conclude that a measurable amount of folding of the interface does occur. A further indication is found

| | $\langle L_t \rangle / \delta$ | $f_\Lambda$ (Hz) | $f_\Lambda \delta / U_\infty$ | $\langle L_t \rangle / L_s$ |
|---|---|---|---|---|
| Present results | 0·46 | 118 | 1·08 | 10·54 |
| Kovasznay *et al.* | 0·60 | 33 | 0·77 | 3·14 |
| Corrsin & Kistler | 1·34 | 50 | 0·39 | 5·05 |
| Antonia & Bradshaw | 0·34 | 535 | 1·52 | 8·00 |

TABLE 5. Burst statistics

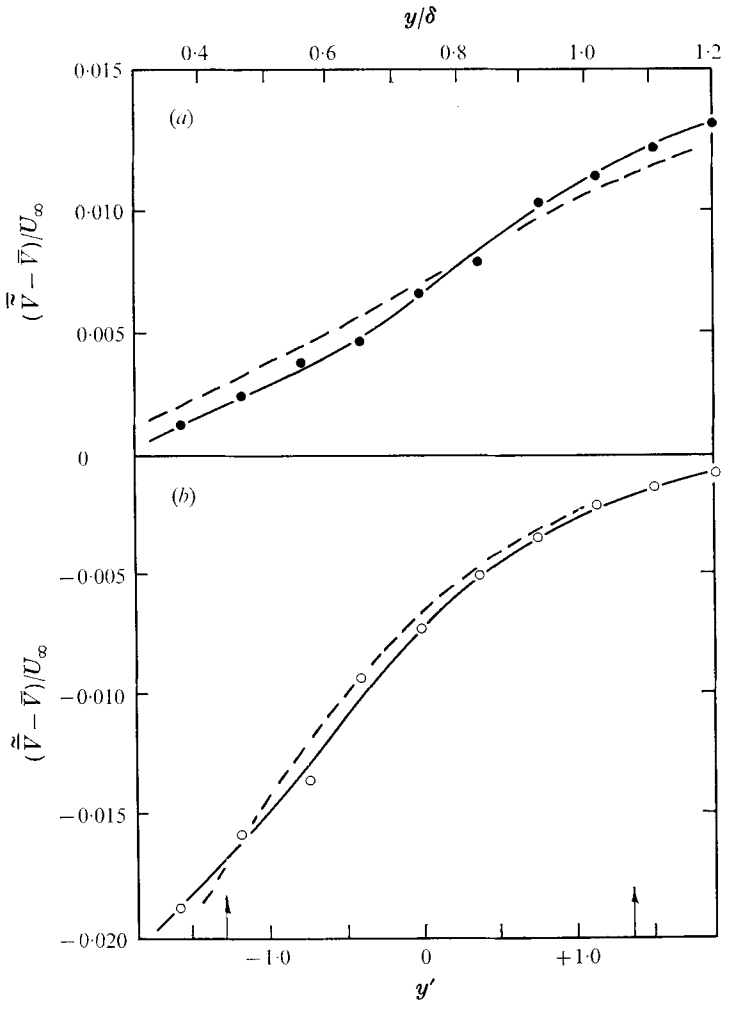


FIGURE 10. Mean lateral velocity in (*a*) turbulent and (*b*) non-turbulent zones. ●, turbulent fluid; ○, non-turbulent fluid; – – –, Kovasznay *et al.* (1970).

by inspecting figure 7. For a normally distributed interface, the functional shape of $L_t$ at a particular position $Y$, say where $\bar{I} = \bar{I}_1$, should be similar to that for $L_n$ at $\bar{I}_2 = 1 - \bar{I}_1$. Clearly this is not so; for example, $L_n$ at $\bar{I} = 0{\cdot}93$ is significantly more peaked than $L_t$ at $\bar{I} = 0{\cdot}04$ and $0{\cdot}10$. In addition, when the ratio of the mean $L_t$ to its value at $I = 0{\cdot}50$ is compared with the ratio expected for a

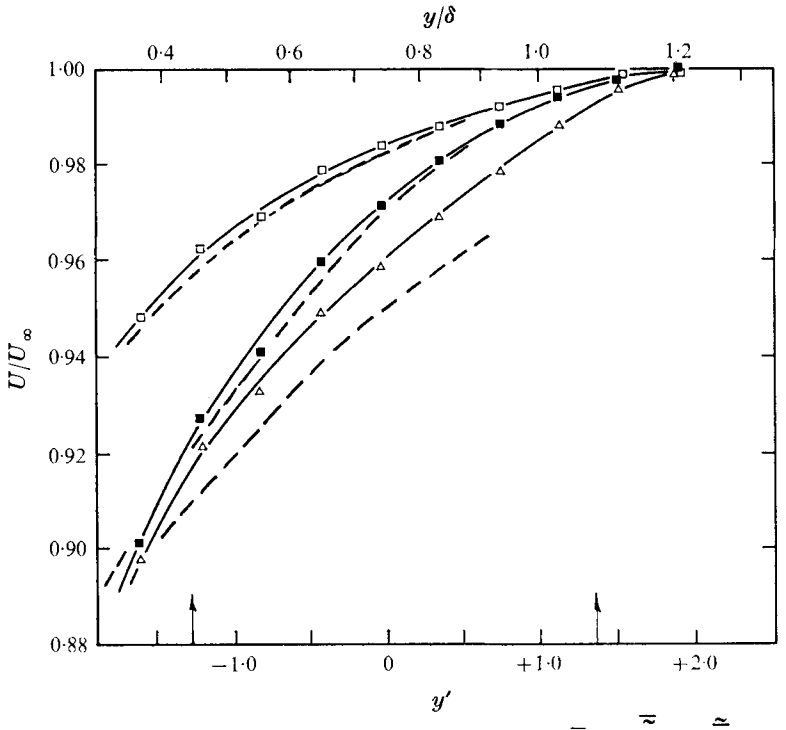


FIGURE 11. Mean streamwise velocity. ■, $\bar{U}$; △, $\bar{\bar{U}}$; □, $\bar{\bar{\bar{U}}}$; ———, Kovasznay *et al.* (1970).

symmetrical Gaussianly distributed surface, the widths at high intermittency levels are found to be too short.

The above remarks must be considered speculative in part since the characteristics of the interface, particularly $f_\Lambda$, are sensitive to decisions on the threshold level and smoothing period. A comparison of the statistics of the bursts at the mean interface position is given in table 5. The relevant variable is $f_\Lambda \delta/U_\infty$ since the burst rate will depend directly upon the mean speed of the flow. The present results are comparable with both those of Kovasznay *et al.* and Antonia & Bradshaw. The last column gives some indication of the smoothing effect in terms of the average burst length $\langle L_t \rangle$.

### 3.2. *Zone mean velocity distributions*

The macroscopic motion of the turbulent and non-turbulent fluid is shown in the next few figures. The transverse component $V$, in figure 10, has been normalized with respect to the total average velocity and indicates typically that the lateral velocity within the turbulent fluid is directed away from the wall throughout the depth of the boundary layer. In the non-turbulent zones this is reversed, the mean velocity being everywhere negative. This is consistent with our physical ideas about the motion of the large entrainment eddies and the data agree well with those of Kovasznay *et al.* (1970), which are shown for comparison. In this and subsequent figures, results of Kovasznay *et al.* are plotted in terms of $y'$ rather than $y/\delta$.

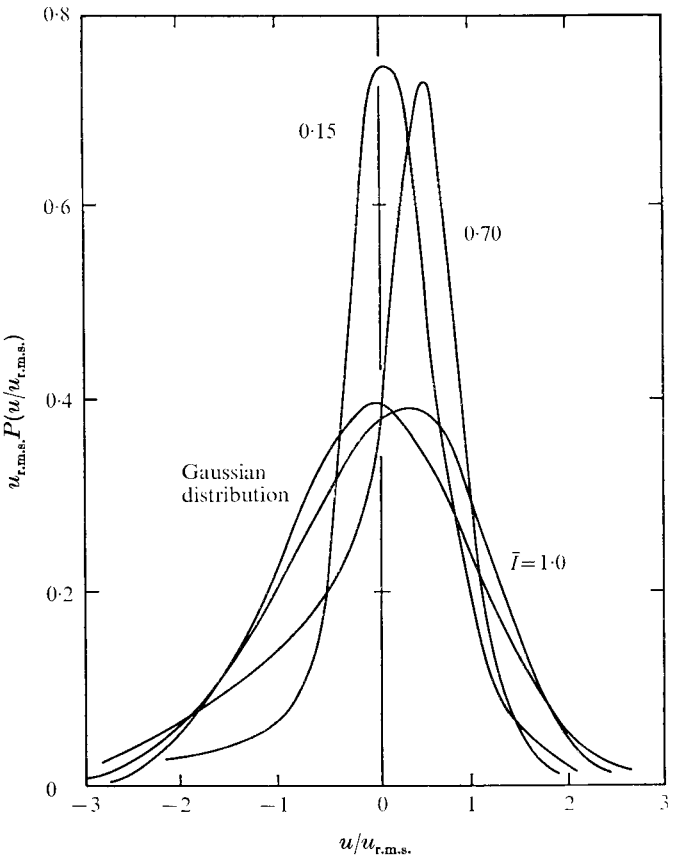


FIGURE 12. Probability density function of the amplitude of the streamwise fluctuating component. Areas normalized to unity.

The streamwise components $U$ are shown in figure 11. Clearly, the fluid within the turbulent regions has, on average, a deficiency of momentum, whereas the non-turbulent fluid, which is sandwiched between the turbulent bulges, has a velocity markedly less than the overall average. It would appear that the irrotational fluid is constrained by pressure forces to move at speeds less than those of the free stream as suggested by Townsend (1970).

### 3.3. *Zone velocity fluctuation intensities*

With the multiplicity of variables in a conditionally sampled flow, one has the option of defining the fluctuating velocity field in a variety of ways. The most meaningful statistical operations are those which compare fluctuations in a given zone or at a specific point so that the corresponding conditional averages of the fluctuations will be zero. For example we note that

$$\overline{\overline{q}}_t(r,t) = 0, \quad \overline{q}_t(r,t) \neq 0,$$

where $q_t = Q(r,t) - \overline{\overline{Q}}(r)$, and the physical interpretation of the latter operation

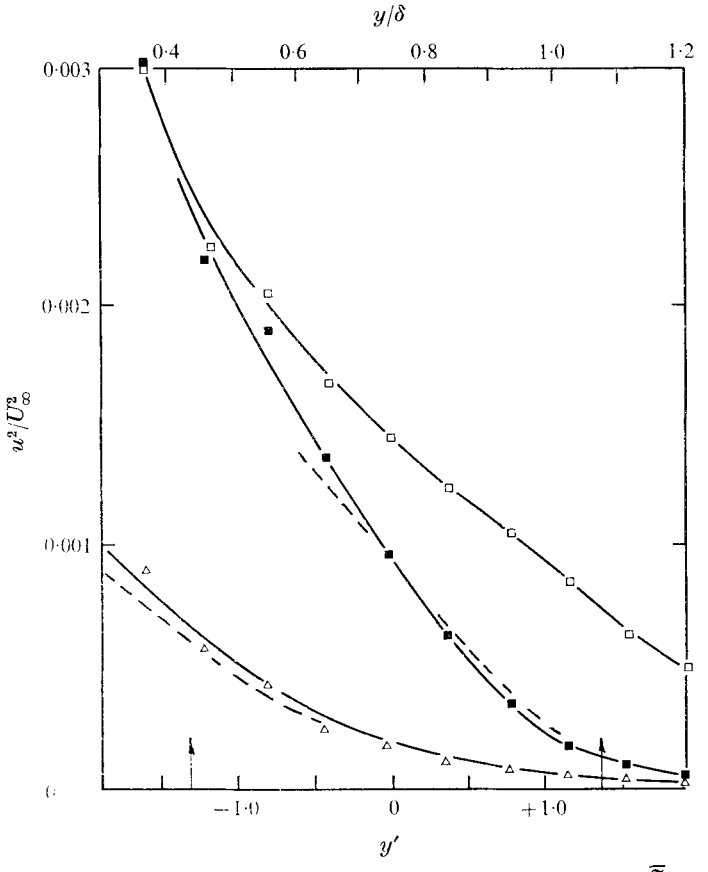


FIGURE 13. Streamwise fluctuating intensitites. ■, $\overline{u^2}$; □, $\tilde{\overline{u_t^2}}$; △, $\tilde{\overline{u_n^2}}$; ---, Kovasznay *et al.* (1970).

is unnecessarily complicated. The conservation statement for the various fluctuation intensities must be related by

$$\overline{q^2} = \bar{I}\tilde{\overline{q^2}} + (1-\bar{I})\,\tilde{\overline{q^2}} = \bar{I}\tilde{\overline{q_t^2}} + (1-\bar{I})\,\tilde{\overline{q_n^2}} + \bar{I}(1-\bar{I})\,(\tilde{\overline{Q}} - \tilde{\overline{Q}})^2$$

and the appropriate operations are defined in table 3.

The streamwise fluctuations relative to the overall mean were measured and the probability density functions of this variable plotted at different points across the boundary layer. Some typical results are shown in figure 12. At high values of the intermittency fraction, i.e. deep within the boundary layer where the fluid is mostly turbulent and therefore more homogeneous, the shape is close to a Gaussian distribution. As the relative proportion of non-turbulent fluid increases, the distributions become more and more peaked and the tails of the distributions correspondingly fatter. Similar characteristics were observed by Antonia & Bradshaw (1971). More recently Frankiel & Klebanoff (1973) have measured this quantity for a number of positions across the boundary layer. The present results show direct quantitative agreement with their data, which exhibited a maximum in the value of $P[u/u_{\text{r.m.s.}}]$ of 0·72 and noticeable positive

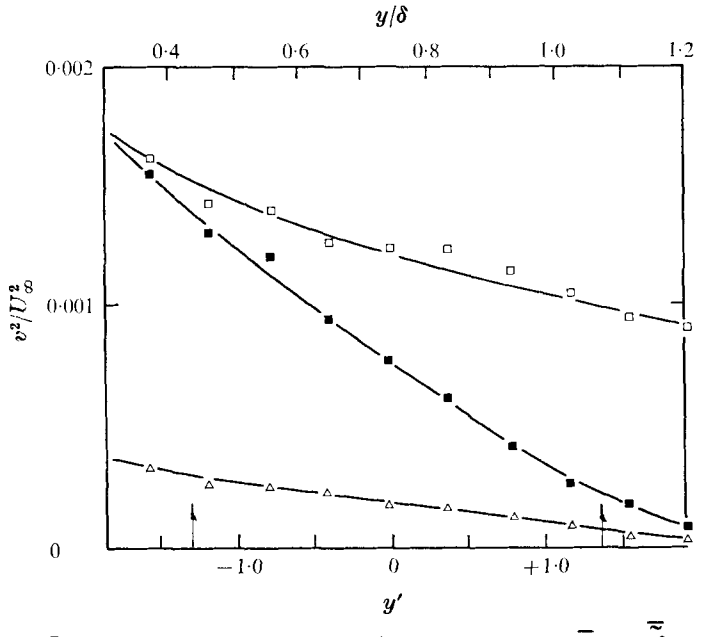


FIGURE 14. Transverse fluctuating intensities. ■, $\overline{v^2}$; □, $\overline{v_t^2}$; △, $\overline{v_n^2}$.

skewness at a position where $\bar{I} = 0{\cdot}59$. Our distribution for $\bar{I} = 0{\cdot}70$ is essentially the same. At increasing distances from the wall they found the eccentricity to diminish until at a point beyond the interface, i.e. within the wholly non-turbulent fluid, the distribution became Gaussian. We did not check this extreme position.

To examine the two fluid domains separately, the conditional averaging was applied to the fluctuating fields. The first four moments characterizing the probability density functions of the streamwise and transverse fluctuation components were evaluated and are shown in the following series of figures. As expected, the variance or second moment (figures 13 and 14) decreases monotonically with distance from the wall. For the $u$ component the intensities are generally low in the non-turbulent zone except well within the boundary layer, where the values start to rise markedly. The agreement with the data of Kovasznay *et al.* is good. The turbulent zones retain a high level of turbulence at the outer edges of the motion, greater than the overall average would lead one to expect. In figure 14 the corresponding values of the $v$ component are plotted. The magnitudes are generally lower than for $u$ but the same general trends are evident. The non-turbulent fluctuations are rather smaller and the averages taken in the turbulent zone tend to be more uniform.

To extend the picture, the zone-averaged skewness factors of the density functions have been plotted in figure 15. The non-zero values reflect the magnitude of the asymmetry of these distributions. In the non-turbulent regions, the $u$ component varies roughly from $+1$ to $-1$ through the boundary layer while within the turbulent zones it remains approximately $-1$. The $v$ components display an entirely different behaviour. Non-turbulent values are effectively zero while

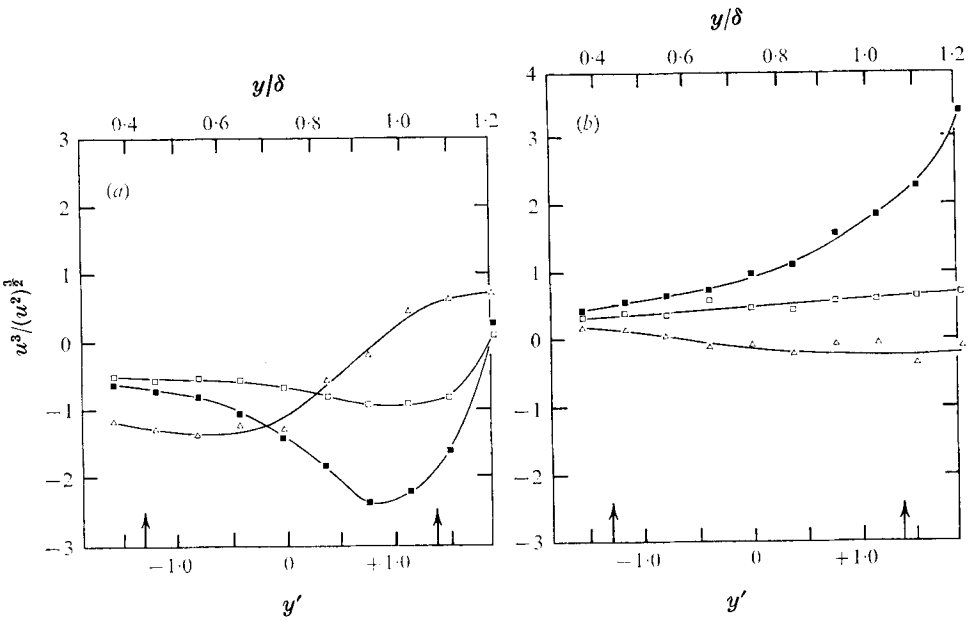


FIGURE 15. Skewness factor of (*a*) streamwise and (*b*) transverse component. ■, overall; □, turbulent; △, non-turbulent.

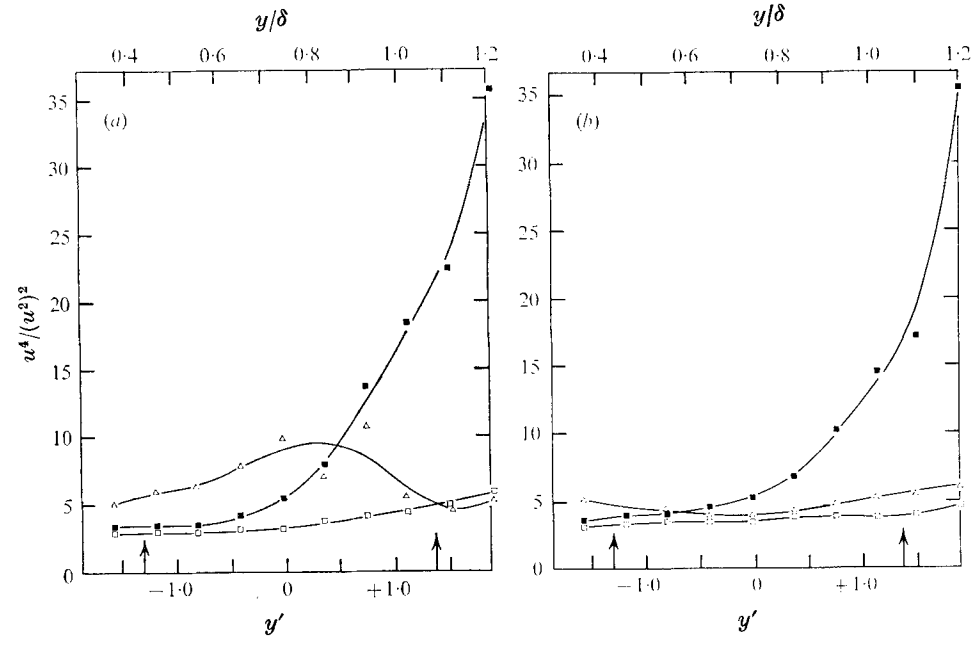


FIGURE 16. Flatness factor of (*a*) streamwise and (*b*) transverse component. ■, overall; □, turbulent; △, non-turbulent.

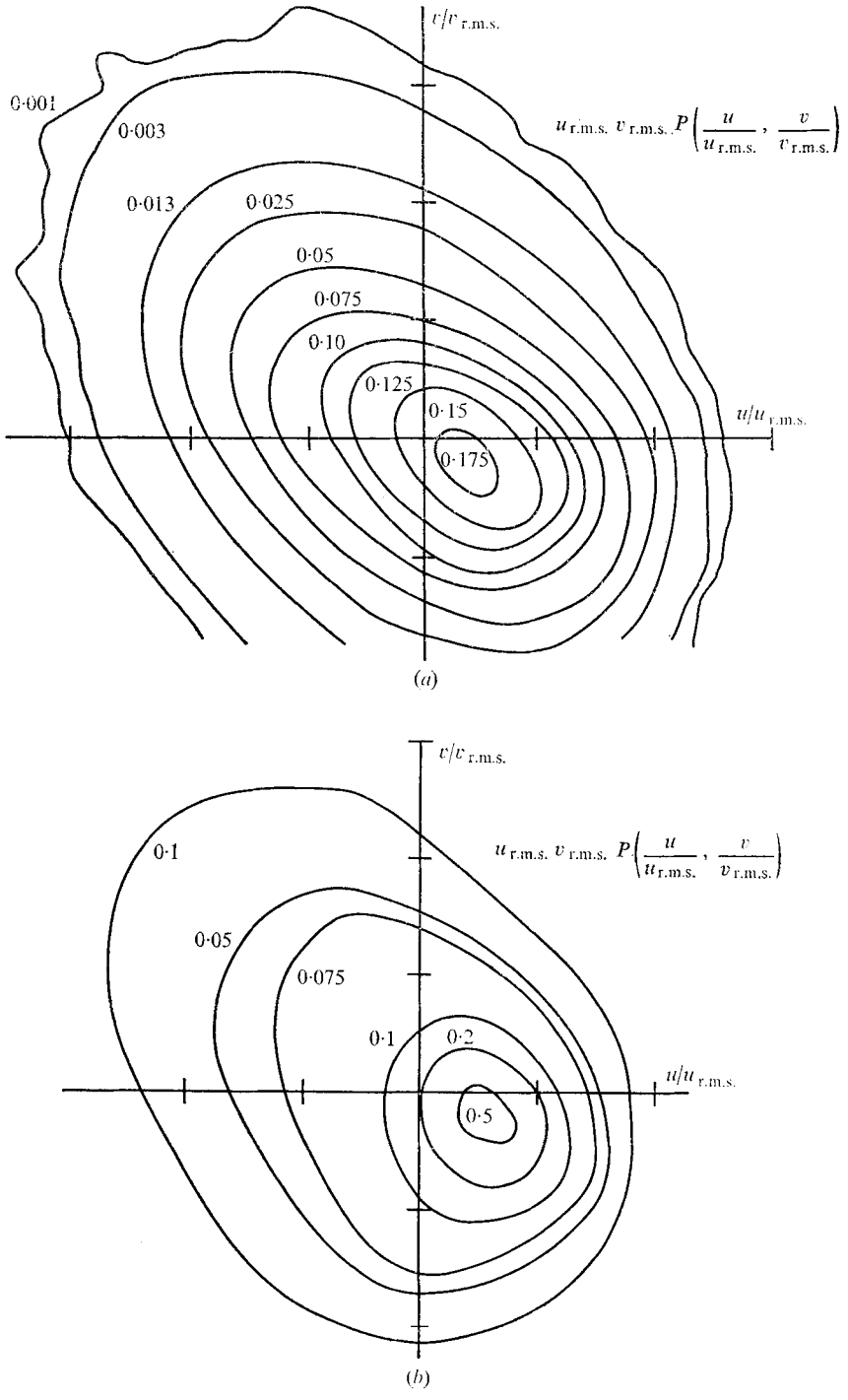


FIGURE 17. Joint probability density of amplitudes of $u$ and $v$ at (*a*) $y/\delta = 0{\cdot}15$, $\bar{I} = 1{\cdot}00$ and (*b*) $y/\delta = 0{\cdot}70$, $\bar{I} = 0{\cdot}30$ (divisions on axes in units of one).

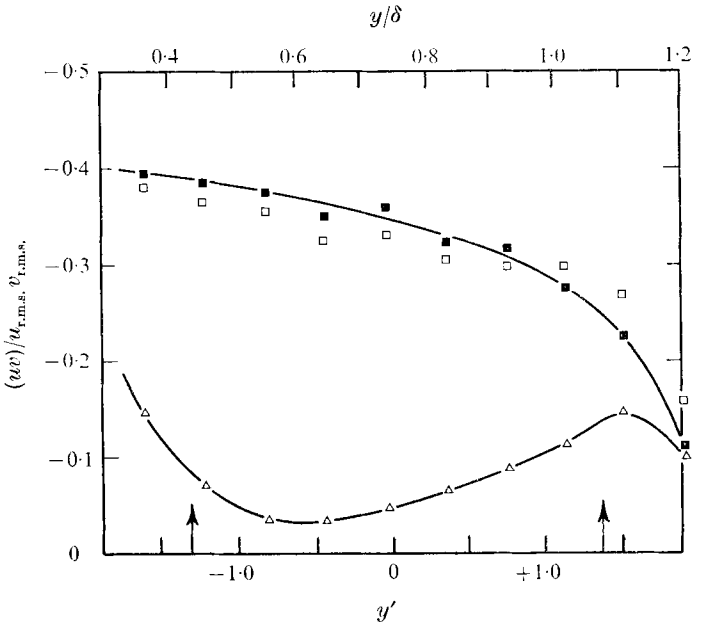


FIGURE 18. Correlation of $u$ and $v$ across the boundary layer. ■, overall; □, turbulent; △, non-turbulent.

averages taken in the turbulent zone lie consistently above the zero line. These results agree well with the data of Antonia (1972), taken at a single point at the outer edge of the boundary layer.

The zone-averaged flatness factors plotted in figure 16 illustrate quite clearly that, within the turbulent zones, the structure of the flow is uniform since both factors are close to the value of 3 expected for a Gaussian distribution. The variability of the flatness factor in the non-turbulent flow is most marked for the $u$ terms. Why this should be so is not clear. The rapid increase in $u^4$ and $v^4$ of course merely reflects the overall inhomogeneous turbulent structure of the outer intermittent edges of the boundary layer. Both $u$ and $v$ components show this accurately. On balance, it would appear that the flatness factor of $v$ rather than $u$ would be a better criterion to measure the effects of the intermittency because of the inconsistent behaviour of $u^4$.

More information on the directional characteristics of the fluctuating field can be obtained by considering the joint probability density functions. We restrict the analysis to two representative positions within the boundary layer,

$$y/\delta = 0{\cdot}15 \quad \text{and} \quad 0{\cdot}70,$$

since the data processing was rather time consuming. The separate constituents of the correlation coefficient were ensemble averaged and then assembled to produce the joint distribution. The contours are shown in figure 17. In each case the point maxima occur in the lower right-hand quadrant, i.e. $u > 0$, $v < 0$, whereas the region of the total greatest probability is displaced into the quadrant $u < 0$, $v > 0$. Wallace, Eckelmann & Brodkey (1972) found that deep within the

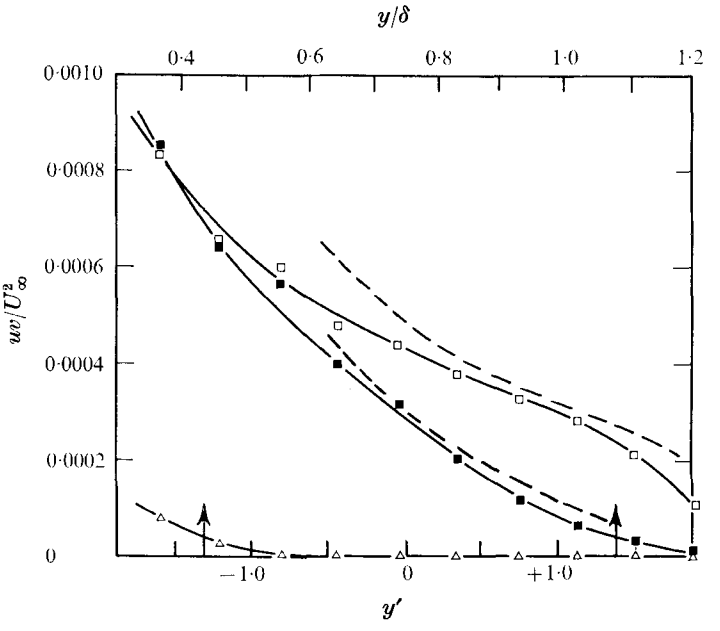


FIGURE 19. Reynolds shear stress. ■, overall; □, turbulent; △, non-turbulent; – – –, Kovasznay *et al.* (1970).

boundary layer these combinations producing positive stress had measurably larger time scales than the motions producing negative stress. This would be consistent with our results if we assumed that the eccentricity of the contours reflects the activity of the larger entrainment eddies in the intermittent region of the boundary layer.

The correlation coefficient was measured independently across the boundary layer and conditionally averaged within the zones. The results are presented in figure 18. As expected, the values in the non-turbulent fluid are very small, while the magnitudes determined in the turbulent zone are essentially equal to the overall averaged values. It is surprising, however, that a distinctive trend can be observed for the non-turbulent data, namely a three-fold increase above the minimum value both deep within the layer and at the outer edges of the flow. The implication here is that the non-turbulent fluctuations must be correlated in regions of strong activity. One would expect perhaps that most of the $\overline{uv}$ energy would occur at the low wavenumber end of the spectrum, i.e. the correlation relates more to $\overline{U}\,\overline{V}$ than to $\overline{uv}$ in the non-turbulent zone. The variation of the absolute value of $\overline{uv}$ is shown in figure 19 along with the results of Kovasznay *et al.*

To supplement the picture, the probability density function of $\overline{uv}$ was measured at a few representative points across the boundary layer with the results shown in figure 20. The distributions are strongly peaked, this effect increasing as we move to the outer regions of the flow where the intermittency is high. This is expected since even the distribution of the product of uncorrelated Gaussian variables shows this characteristic (Antonia, Atkinson & Luxton 1973). As well, a marked skewness is evident for all positions through the boundary layer. A similar

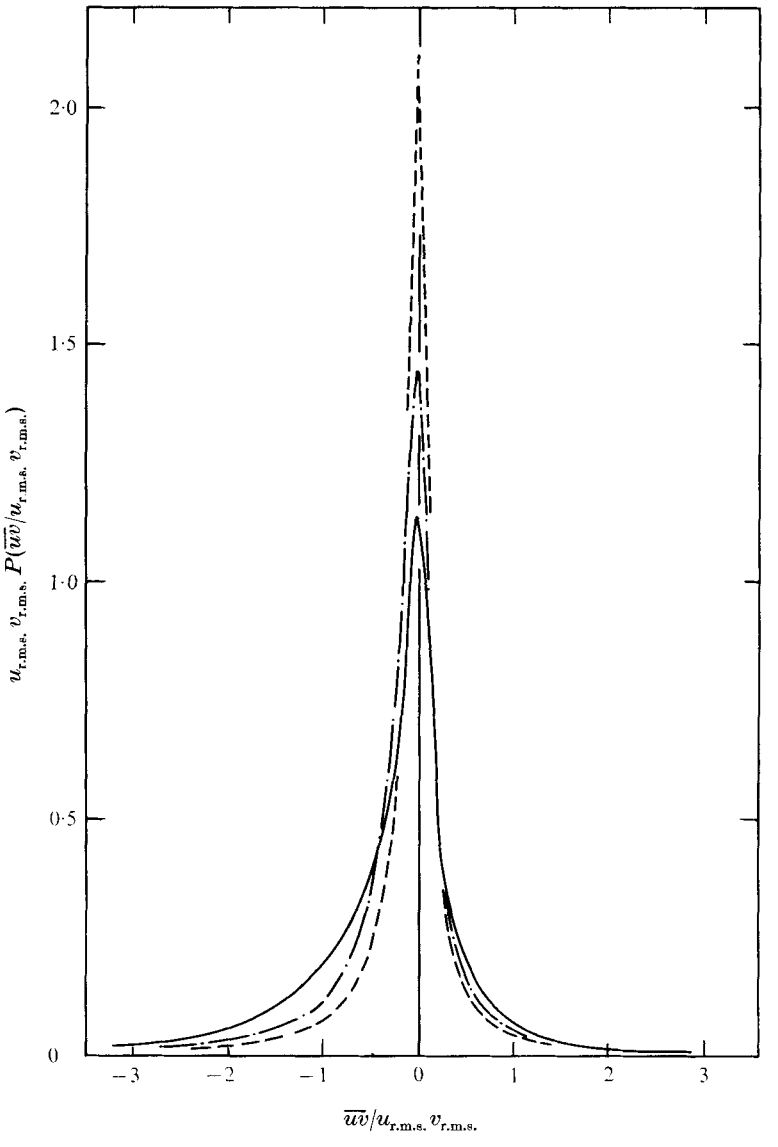


FIGURE 20. Probability density function of amplitudes of $uv$. ——, $y/\delta = 0{\cdot}94$, $\bar{I} = 0{\cdot}15$; – – –, $y/\delta = 0{\cdot}70$, $\bar{I} = 0{\cdot}30$; – · – · –, $y/\delta = 0{\cdot}15$, $\bar{I} = 1{\cdot}0$. Areas normalized to unity.

result was found by Gupta & Kaplan (1972), who evaluated the third moment of $\overline{uv}$. Their data showed a dependence upon Reynolds number in the very outer regions. The skewness increased rapidly beyond $y^+ = 400$ ($y/\delta = 0{\cdot}15$ is approximately equivalent to $y^+ = 760$ for our flow) for $Re_{\delta_2} = 1900$. This did not occur with the higher $Re_{\delta_2}$ of 6500. Thus our results at $Re_{\delta_2} = 9700$ would not, presumably, be expected to show the large increase in skewness.

The various triple products of the velocity fluctuations were extracted from the data records to give some indication of the intensity of the turbulent convective

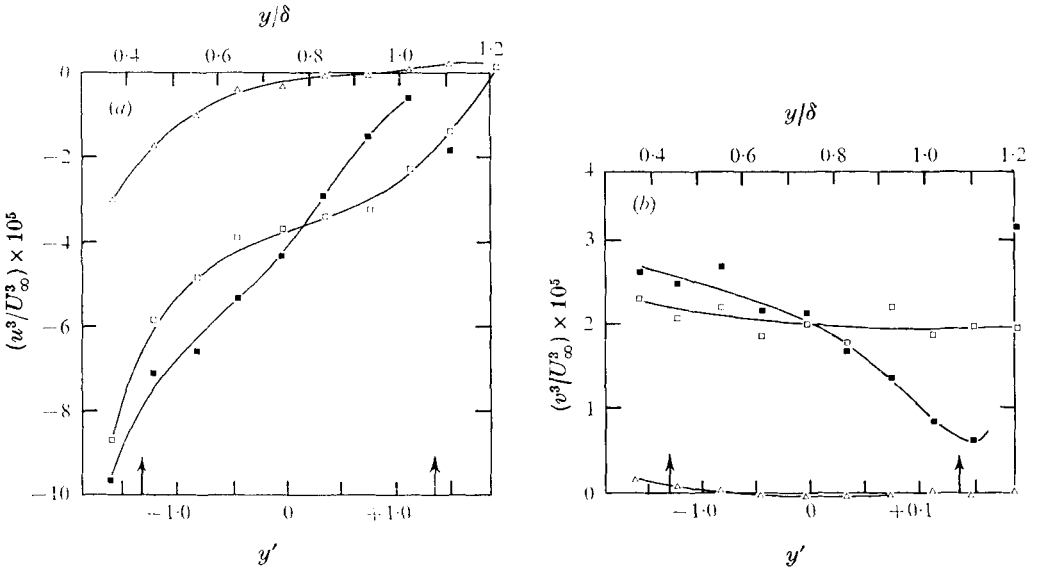


FIGURE 21. Third-order fluctuation intensity for (*a*) $u$ and (*b*) $v$. ■, overall; □, turbulent; △, non-turbulent.

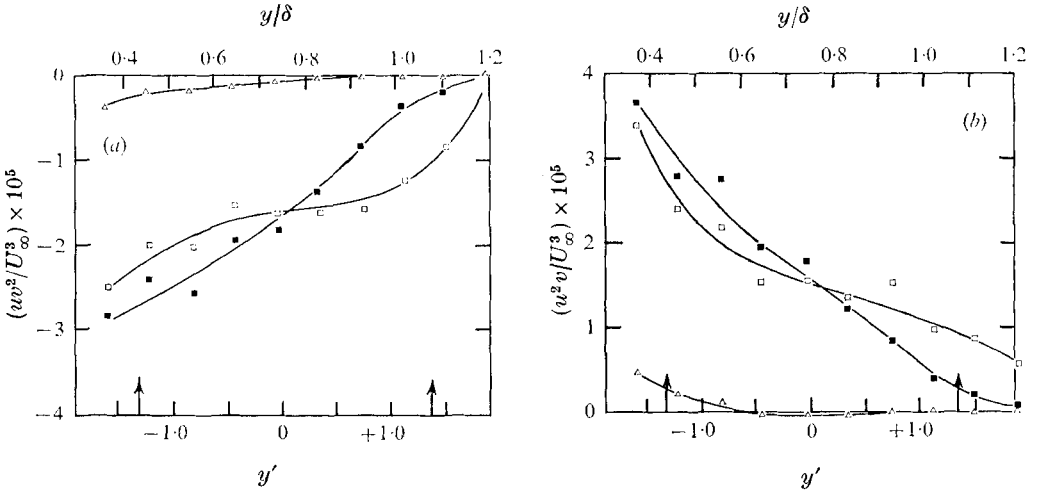


FIGURE 22. Third-order cross-products (*a*) $uv^2$ and (*b*) $u^2v$. ■, overall; □, turbulent; △, non-turbulent.

terms. The variation in the third moments, $u^3$ and $v^3$, is shown in figure 21. The large magnitude of the $\overline{u}^3$ and $\overline{u_t^3}$ terms, compared with the respective transverse terms, suggests that it would be erroneous to eliminate the streamwise components when considering any balance of kinetic energy. Wygnanski & Fiedler (1970) reported similar, surprisingly large magnitudes for these components in a mixing layer.

The conventional, turbulent and non-turbulent zone averages of the triple cross-products are shown in figure 22. Within the non-turbulent regions, diffusive

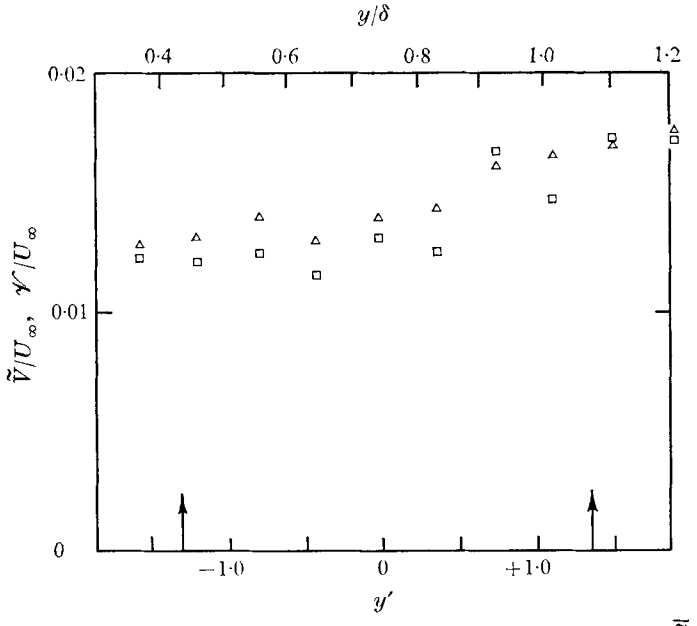


FIGURE 23. Lateral bulk convection velocities. □, $\mathscr{V}$; △, $\tilde{\bar{V}}$.

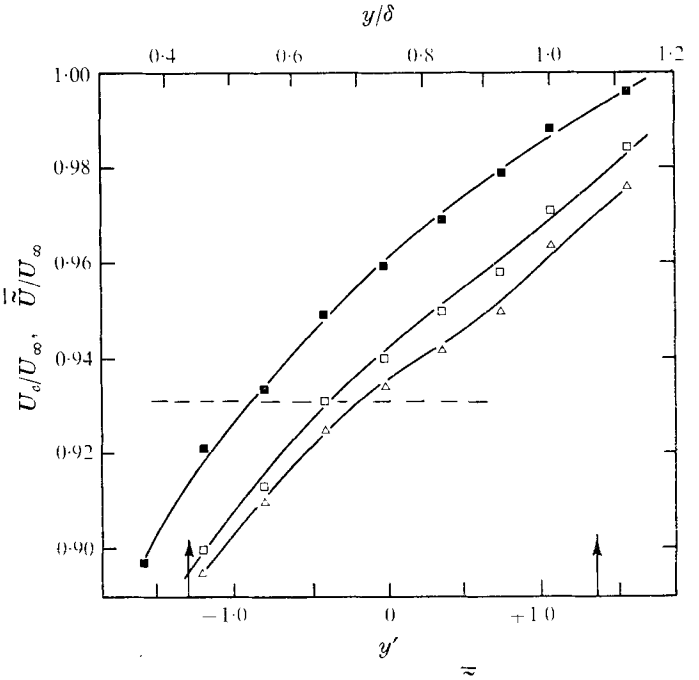


FIGURE 24. Streamwise convection velocities. ■, $\tilde{\bar{U}}$; △, $U_c$ based on transport of $u_t^2$; □, $U_c$ based on transport of $q_t^2$; – – –, mean value, Kovasznay *et al.* (1970).

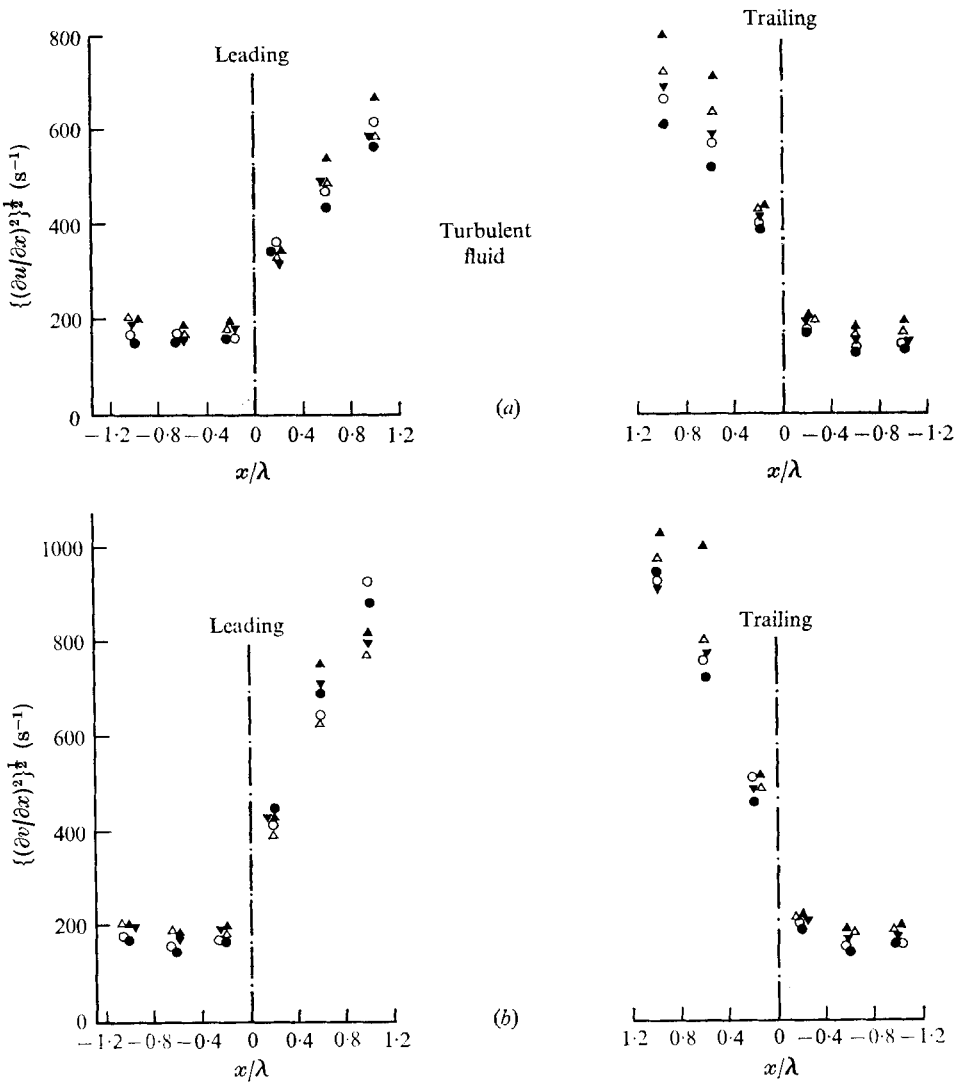


FIGURES 25 (*a*) and (*b*). For legend see facing page.

action must be negligible. The data verify this satisfactorily, the non-turbulent averages being effectively zero. We see that turbulent diffusion is directed outward, away from the wall and in an upstream direction.

As an approximation we may write the turbulent kinetic energy as

$$\tfrac{1}{2}\tilde{\tilde{q}}_t^2 = 3(\tilde{\tilde{u}}_t^2 + \tilde{\tilde{v}}_t^2).$$

With this then it is possible to define a bulk convection velocity in the form

$$\mathscr{V}_t = \tilde{\bar{g}}/\tilde{\bar{q}}_t, \quad g \equiv v_t q_t^2.$$

This quantity was evaluated and compared with the lateral mean transverse velocity $\tilde{\tilde{V}}$ in the turbulent fluid with the results shown in figure 23. It is seen

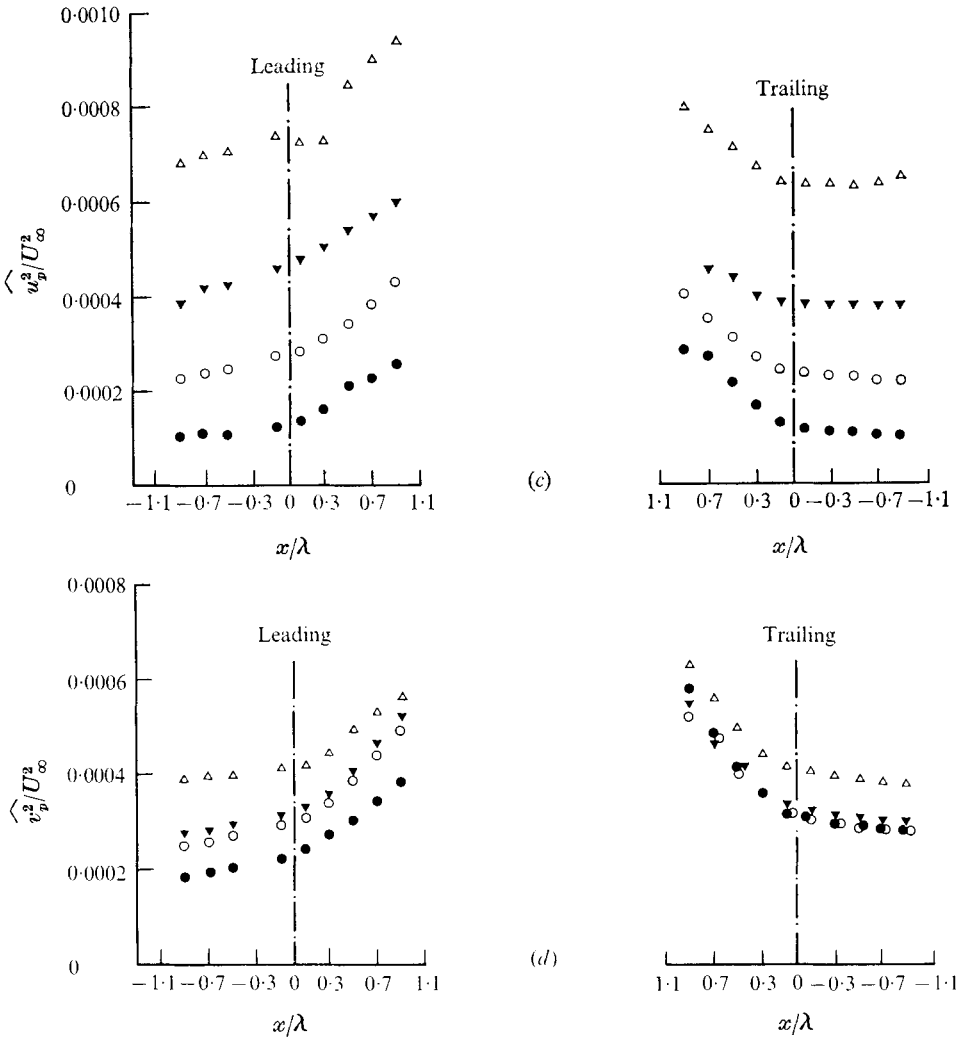


FIGURE 25. Distribution of (*a*) $\partial u/\partial x$, (*b*) $\partial v/\partial x$, (*c*) $u_p^2$ and (*d*) $v_p^2$ across the turbulent interface. ●, $y' = \pm 1{\cdot}4$, $\bar{I} = 0{\cdot}10$; ○, $y' = \pm 0{\cdot}8$, $\bar{I} = 0{\cdot}24$; ▼, $y' = 0$, $\bar{I} = 0{\cdot}51$; △, $y' = -0{\cdot}8$, $\bar{I} = 0{\cdot}78$; ▲, $y' = -1{\cdot}4$, $\bar{I} = 0{\cdot}93$.

that the data are essentially the same. Bulk convection by the large entrainment eddies is the major transport mechanism in the outer region of the flow. The gradient diffusion processes are negligibly small. A value of $\mathscr{V}/U$ of about this magnitude was found by Townsend (1956, p. 147) for the outer edge of the two-dimensional turbulent wake.

The streamwise convection velocity can be estimated from third-order quantities involving $u$ fluctuations,

$$U_c = \bar{\bar{U}} + \bar{\bar{u_t^3}}/\bar{\bar{u_t^2}},$$

or the streamwise transport of turbulent energy,

$$U_c = \bar{\bar{U}} + \bar{\bar{h}}/\bar{\bar{q_t^2}}, \quad h \equiv u_t q_t^2.$$

These definitions give almost the same result, see figure 24, the values lying slightly below those for the average velocity within the turbulent zones. Essentially, the bulges are translating in the main direction of the flow at $U_c = \overline{\overline{U}}$. The mean value of Kovasznay *et al.* (1970) is shown for comparison.

### 3.4. *The variation across the turbulent interface*

A region within two Taylor microscales either side of the turbulent/non-turbulent interface region was examined. Whenever an upstream or downstream edge of a turbulent zone was detected, point values of the mean and turbulent velocities, derivatives, etc., were taken relative to the position of the interface. This was continued for a long enough length of record so that stable ensemble averages resulted. The data processing was repeated for specific stations throughout the depth of the boundary layer and the results appear in a series of plots starting with figure 25(*a*). The diagrams have been arranged to represent a time trace moving from left to right. Thus the data on the left are for the leading edge or front of the turbulent bulge (the downstream portion), while those on the right describe the variation through the trailing edge or back (the upstream edge). Each symbol refers to a particular distance from the wall in terms of the non-dimensional co-ordinate $y'$. All data are normalized with respect to the micro-scale $\lambda$, rather than specifying it relative to the width of the turbulent bursts as was done for example by Antonia & Bradshaw (1971) and Antonia (1972). This gives an absolute measure of the change in variables through the interface.

As expected, derivatives of the velocity components, as seen in figures 25(*a*) and (*b*), increase sharply across the turbulent front. Although self-similar behaviour within the non-turbulent region is evident, the data within the turbulent burst show marked scatter. This is somewhat surprising, since it was observed by Antonia & Bradshaw that the velocity distribution within bulges was self-similar when plotted over an ensemble of the non-dimensional turbulent bursts. The rapid rise of the magnitude of the derivatives, especially $\partial v/\partial x$, reflects the intensity of the vortical fluctuations. Further into the turbulent zone, the data must approach some state of homogeneity, since previous work suggests that most of the fine structure within bursts is uniform. The present data are representative of the interface only.

In contrast, the changes in the intensity fluctuations shown in figures 25(*c*) and (*d*) are marked by a more gradual transition. For each component the trailing edge shows a discernible change across the front, although not as marked as with the gradient results in the previous figures. Constant and rather large values of the intensity occur in the non-turbulent zone immediately outside. The data for the leading edge of the bulge for both $u$ and $v$ show a monotonic drop through the interface, however. Although Antonia (1972) did not make direct measurements through the turbulent front, his data, taken at $\bar{I} = 0{\cdot}19$, for the turbulent and non-turbulent zones are in general agreement with the present results. Large slopes in $\widehat{u_p^2}$ and $\widehat{v_p^2}$ can be seen at the edges of his bursts. In the non-turbulent zones the intensity is uniform and close to zero. Quantitative comparisons are difficult however, because of the different methods of plotting the results. At most, the comparison is valid only in the immediate region of the interface.

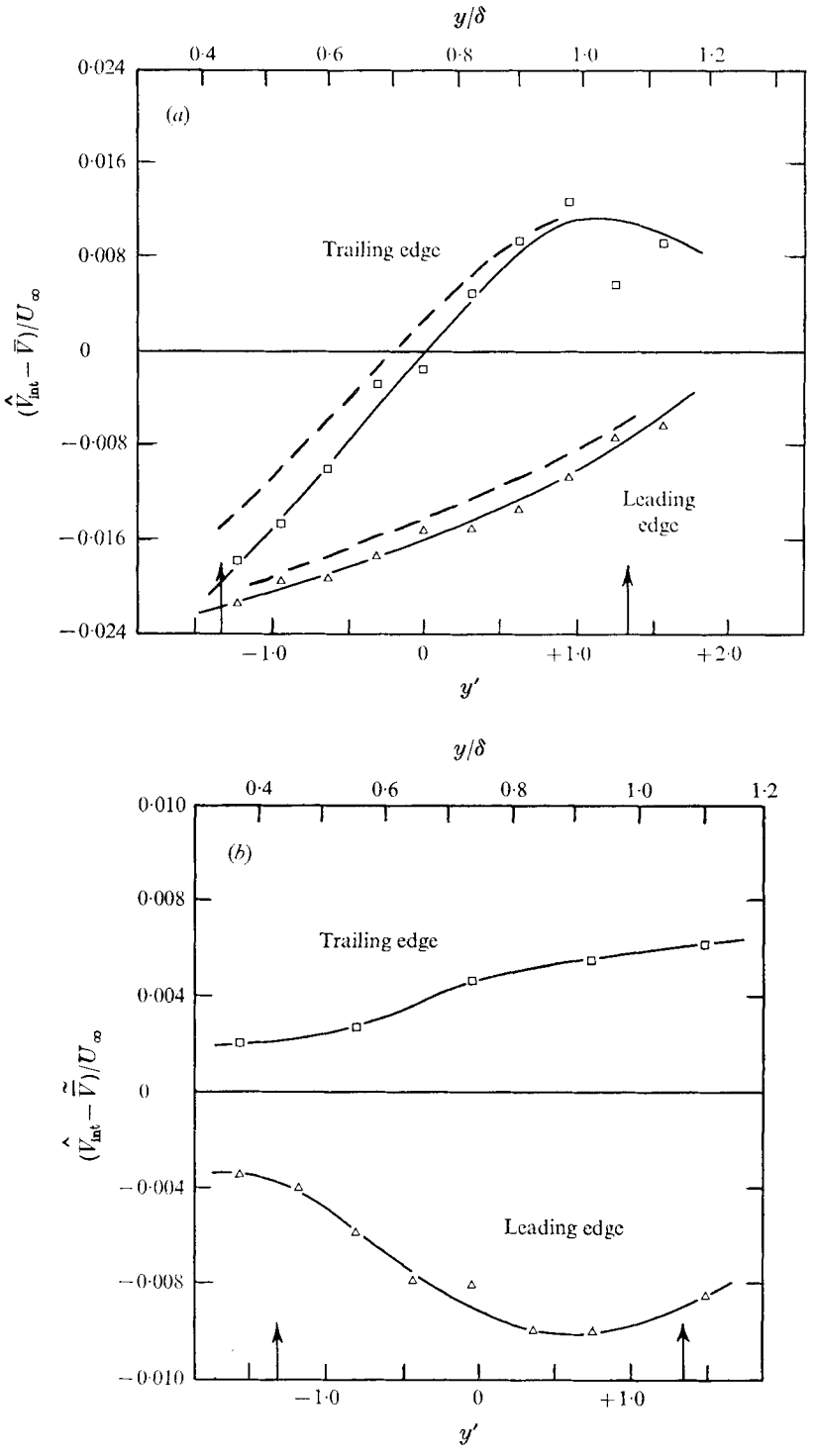


FIGURE 26. Mean transverse velocity at the turbulent interface
–––, Kovasznay *et al.* (1970).

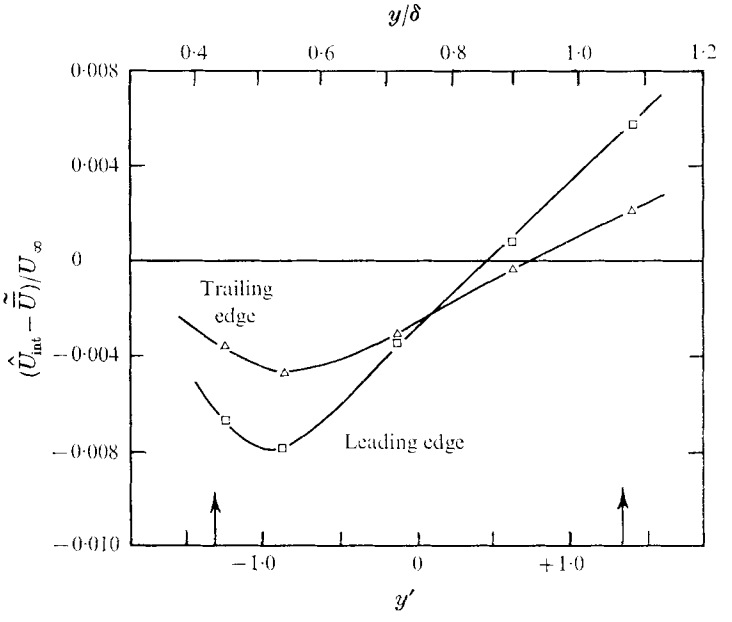


FIGURE 27. Mean streamwise velocity at the turbulent interface.

The average transverse fluid velocity at the interface position is plotted relative to the overall average $\overline{V}$ in figure 26 (*a*). As well, the results of Kovasznay *et al.* are included for comparison. They have interpreted the change of sign which occurs at the trailing edge as an apparent stagnation point as the non-turbulent fluid encounters the back of the turbulent bulge and splits. We explored this behaviour more closely by relating the point-average velocity $\hat{V}_{int}$ to $\tilde{\overline{V}}$, the average taken in the non-turbulent fluid, which appears physically more meaningful. The result is shown in figure 26 (*b*), where it can be seen that the conditions for such a stagnation point do not exist. Evidently the non-turbulent fluid at the back of the eddy remains roughly unidirectional with an outward vertical component. Together with the negative value of $\hat{V}_{int}$ at the leading edge, we are able to infer a convecting action, similar to a couple, which causes the eddy to rotate in the direction of the mean strain field.

The average streamwise velocity at the interface was determined and is plotted in figure 27. These results suggest an interesting behaviour. In the outer zone, beyond about $\overline{Y}$, the eddies grow in length as the leading edge moves away, relatively, from the trailing edge. However, deeper into the layer, the role is reversed and the edges approach one another. The implication is that the average eddy undergoes a pinching effect brought on by the inrush of non-turbulent fluid into the interior. In the outer regions, where the bulges are convected along more or less at the velocity of the free stream, a spreading of the eddy (in the streamwise direction) occurs as the interface expands into the non-turbulent fluid. These results are different from those of Kaplan & Laufer (1968) and Antonia & Bradshaw (1971), who found $U_{int}$ (leading) $- U_{int}$ (trailing) to be positive everywhere although of small magnitude.

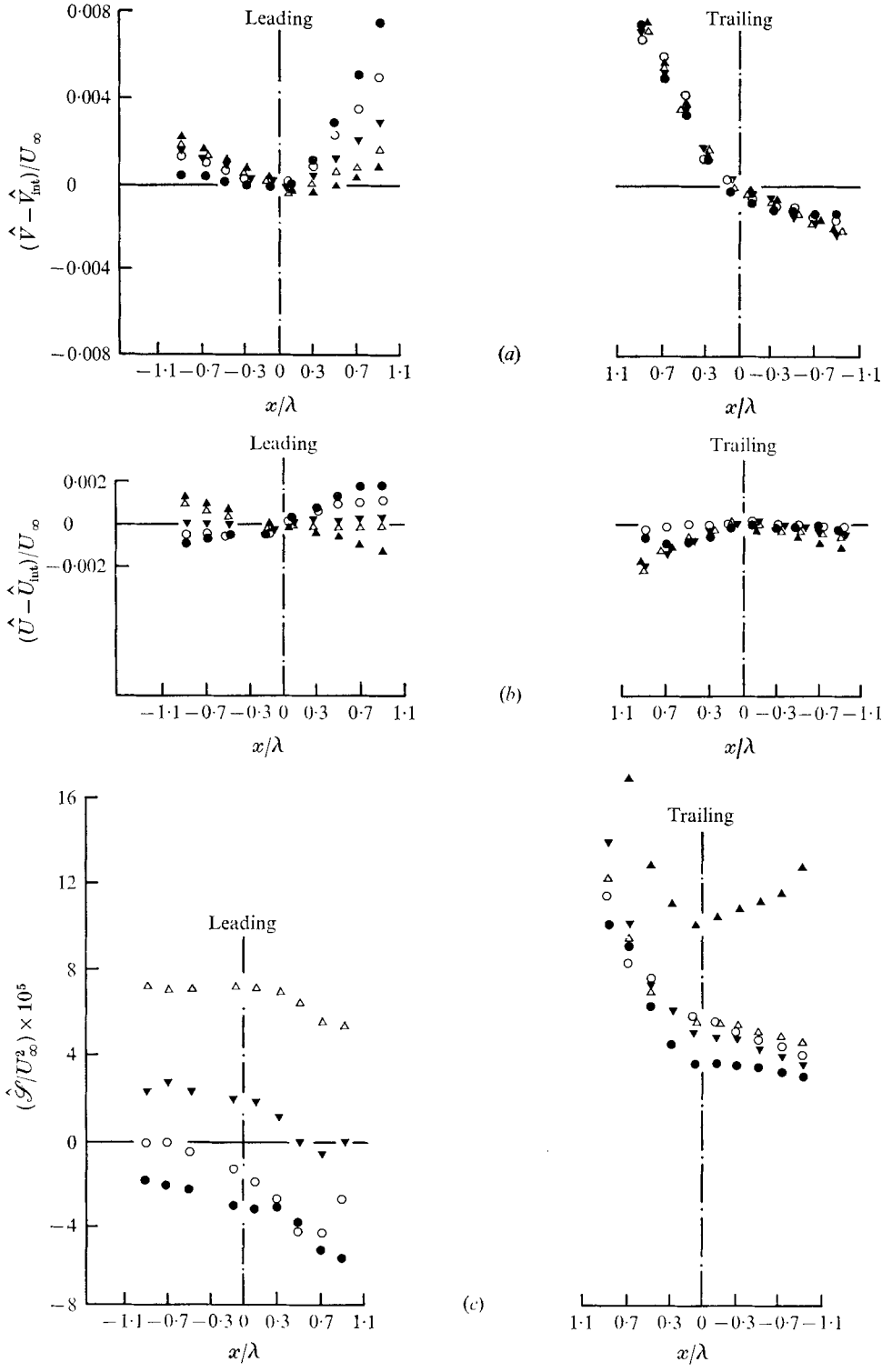


FIGURE 28. Distribution of (*a*) mean transverse velocity, (*b*) mean streamwise velocity and (*c*) Reynolds stress across the interface. Symbols as in figure 25.

The change in sign of $\hat{U}_{\text{int}}$ for both leading and trailing edge, through the depth of the boundary layer, is consistent with the results of the previous figure, in that the eddy is being sheared or twisted by the mean velocity field.

The variations of mean velocity components through the interface were evaluated next. Figure 28(*a*) shows the behaviour of the transverse velocity component. The observed increase in mean velocity as we move into the burst supports the previous results in that there is a strong mean outward movement within the turbulent zone. At the trailing interface, there is complete self-similarity of the velocity profile. Furthermore, the gradient $\partial \hat{V}/\partial x$, although changing sharply across the front, remains non-zero in the non-turbulent fluid. The results for the leading edge show no similar trend. The distribution of the $U$ component (figure 28*b*) exhibits a generally unremarkable behaviour and it would appear that the mean velocity field, with the single exception of $\hat{V}$ at the trailing edge, is continuous through the interface.

Some final measurements are presented in figure 28(*c*), where we see the point values of the turbulent Reynolds stress variation across the interface. These show a peculiar contrast. At the trailing edge, the change in magnitude is distinct (with the exception of a position deep within the boundary layer). The picture is decidedly different at the leading edge, where the change is almost imperceptible. Furthermore, in the outer regions of the flow, the sign of the stress $\hat{\mathscr{S}}$, where $\mathscr{S} \equiv u_p v_p$, at this front becomes negative. The loss of definition at the leading edge of the burst is unexpected since the vortical fluctuations in this region, as indicated by the behaviour of $(\partial v/\partial x)^2$ say in figure 25(*a*), show a marked change. Such quantities are representative of the fine-scale structure however, and it is possible that we see here an effect which is a consequence of the larger scales of the motion. We note that this result was not observed by Antonia (1972). His average burst displayed symmetry of $\hat{\mathscr{S}}$ within the turbulence.

## 4. Discussion

The examination of the interface has shown that significant differences exist in the characteristics of the leading and trailing edges of the turbulent bulges. The back of an eddy exhibits generally sharp changes through the interface of the intensity components and their derivatives. This is also observed, surprisingly, for the lateral mean velocity component $\hat{V}$. In contrast, the front edge exhibits a more diffuse behaviour which shows up most clearly in the measurements of $\hat{\mathscr{S}}$. We can infer a reasonable physical picture from these results. As the non-turbulent fluid sweeps up over the back of a turbulent eddy, it strains the interface or superlayer while accelerating it downstream. Gradient changes through the interface will thus be sharp as we in fact have observed. If then, at the front of the burst, a separation of non-turbulent fluid takes place, a wake region will develop on the leading edge. Consequently, changes in the intensity components through this interface will be comparatively small, which again is consistent with our data.

A further comment on the gradient change of $\hat{V}$ which we found at the back of any eddy may be made. In the non-turbulent fluid, close to the interface,

$\partial \hat{V}/\partial x$ was measurably non-zero. This may be suggested as evidence of a layer of mean vorticity in the region immediately outside the turbulent burst. Such a concept was originally proposed by Corrsin & Kistler (1955) in their model of a superlayer and it is physically attractive. A more definite statement would require of course a simultaneous measurement of $\partial \hat{U}/\partial y$ as well as the instantaneous slope of the interface. For this we would have needed an array of probes capable of spatial differentiation, which was beyond the scope of our present investigation.

A generally consistent picture of the large-scale motions of the boundary-layer flow now exists. The entrainment eddies appear to be spatially constrained as a series of individual, randomly occurring events having the mean features described above. In contrast, the intermittent region of a wake exhibits a pattern of growth and decay with marked periodic structure (Grant 1958; Keffer 1965). Although certain ultimate differences in the outer regions of these two flows can be explained, how the large structures develop initially is still an intriguing and debatable point. Townsend (1970) suggests that the differences are a result of an interfacial instability in the case of the wake, a mechanism which is not present to any significant extent in the wall-constrained flow of the boundary layer. Nevertheless, it has become apparent that no steady continuous transfer of energy from the mean motion to the turbulence takes place in either the free or the wall flow. In the case of the boundary layer, for smooth walls, it has been shown conclusively that a bursting or triggering process with origin in the viscous sublayer is established. One would expect that any pattern of internal bursting activity reaching or forming a portion of the boundary between the turbulent and non-turbulent fluid should stand out in contrast to the relatively quiet environment of the non-turbulent medium. We might thus consider the larger zones of turbulence as end products of a combination of interior bursting, subsequent growth, diffusion and possibly, mild interface instability. An analysis of data by Laufer & Narayanan (1971) shows that motions occurring near the viscous sublayer can be scaled with the outer flow parameters.

Nevertheless, a complete connexion has yet to be made. If indeed a relation between inner sublayer bursting and outer entrainment-eddy activity exists in the smooth-wall boundary layer, the physics must be different for the rough-wall case, where inner bursting does not exist. As well, with a turbulence decision tied to the fine structure of the flow, as in our present case, any high frequency burst pattern may be a reflexion of the spectral intermittency rather than the true interfacial bulges (Hedley & Keffer 1974). The lognormal distribution of the short zones of turbulent and non-turbulent flow found in this present study are perhaps a necessary but not sufficient condition for establishing a connexion between the inner and outer motions. We note finally (Oboukov 1962) that the distribution of a large number of positive functions can be represented, at least in the first few moments, by lognormal functions.

This research was sponsored by the National Research Council of Canada, Grant A-2746, and by the Pulp and Paper Research Institute of Canada.

## REFERENCES


ANTONIA, R. A. 1972 *J. Fluid Mech.* **56**, 1.

ANTONIA, R. A., ATKINSON, J. D. & LUXTON, R. E. 1973 *Phys. Fluids*, **16**, 956.

ANTONIA, R. A. & BRADSHAW, P. 1971 *Imp. College Aero. Rep.* no. 71-04.

CORINO, E. R. & BRODKEY, R. S. 1969 *J. Fluid Mech.* **37**, 1.

CORRSIN, S. & KISTLER, A. L. 1955 *N.A.C.A. Rep.* no. 1244.

FIEDLER, H. E. & HEAD, H. R. 1966 *J. Fluid Mech.* **25**, 719.

FRANKIEL, F. N. & KLEBANOFF, P. S. 1973 *Phys. Fluids*, **16**, 725.

GRANT, H. L. 1958 *J. Fluid Mech.* **4**, 149.

GUPTA, A. K. & KAPLAN, R. E. 1972 *Phys. Fluids*, **15**, 981.

HEDLEY, T. B. & KEFFER, J. F. 1974 *J. Fluid Mech.* **64**, 625.

KAPLAN, R. E. & LAUFER, J. 1968 *Proc. 12th Int. Cong. Appl. Mech., Stanford.*

KEFFER, J. F. 1965 *J. Fluid Mech.* **22**, 135.

KENNEDY, D. A. & CORRSIN, S. 1961 *J. Fluid Mech.* **10**, 366.

KIM, H. T., KLINE, S. J. & REYNOLDS, W. C. 1971 *J. Fluid Mech.* **50**, 133.

KLEBANOFF, P. S. 1955 *N.A.C.A. Rep.* no. 1247.

KLEBANOFF, P. S. & DIEHL, Z. W. 1953 *N.A.C.A. Tech. Note*, no. 2475.

KOVASZNAY, L. S. G., KIBENS, V. & BLACKWELDER, R. F. 1970 *J. Fluid Mech.* **41**, 283.

LAUFER, J. & NARAYANAN, M. A. 1971 *Phys. Fluids*, **14**, 182.

LUMLEY, J. L. & PANOFSKY, H. A. 1964 *The Structure of Atmospheric Turbulence.* Interscience.

NARAHARI RAO, K., NARASIMHA, R. & NARAYANAN, M. A. 1971 *J. Fluid Mech.* **48**, 339.

OBOUKOV, A. M. 1962 *J. Fluid Mech.* **13**, 77.

SHEIH, C. M., TENNEKES, H. & LUMLEY, J. L. 1971 *Phys. Fluids*, **14**, 201.

TOWNSEND, A. A. 1948 *Austr. J. Sci. Res.* **1**, 161.

TOWNSEND, A. A. 1956 *The Structure of Turbulent Shear Flow.* Cambridge University Press.

TOWNSEND, A. A. 1966 *J. Fluid Mech.* **26**, 689.

TOWNSEND, A. A. 1970 *J. Fluid Mech.* **41**, 13.

WALLACE, J. M., ECKELMANN, H. & BRODKEY, R. S. 1972 *J. Fluid Mech.* **54**, 39.

WYGNANSKI, I. & FIEDLER, H. E. 1970 *J. Fluid Mech.* **41**, 327.